Lithos 210–211 (2014) 224–241

Contents lists available at ScienceDirect

Lithos

journal homepage: www.elsevier.com/locate/lithos

Sabzevar Ophiolite, NE Iran: Progress from embryonic oceanic lithosphere into magmatic arc constrained by new isotopic and geochemical data

Hadi Shafaii Moghadam [a,*], Fernando Corfu [b], Massimo Chiaradia [c], Robert J. Stern [d], Ghasem Ghorbani [a]

[a] School of Earth Sciences, Damghan University, Damghan 36716-41167, Iran
[b] Department of Geosciences, University of Oslo, Blindern, N-0316 Oslo, Norway
[c] Département de Minéralogie, Université de Genève, Genève, Switzerland
[d] Geosciences Department, University of Texas at Dallas, Richardson, TX 75083-0688, USA

ARTICLE INFO

Article history:
Received 30 April 2014
Accepted 13 October 2014
Available online 22 October 2014

Keywords:
Late Cretaceous
U–Pb zircon
Radiogenic isotopes
Supra-subduction zone
Sabzevar ophiolite
Iran

ABSTRACT

The poorly known Sabzevar–Torbat-e-Heydarieh ophiolite belt (STOB) covers a large region in NE Iran, over 400 km E-W and almost 200 km N-S. The Sabzevar mantle sequence includes harzburgite, lherzolite, dunite and chromitite. Spinel Cr# (100Cr/(Cr + Al)) in harzburgites and lherzolites ranges from 44 to 47 and 24 to 26 respectively. The crustal sequence of the Sabzevar ophiolite is dominated by supra-subduction zone (SSZ)-type volcanic as well as plutonic rocks with minor Oceanic Island Basalt (OIB)-like pillowed and massive lavas. The ophiolite is covered by Late Campanian to Early Maastrichtian (~75–68 Ma) pelagic sediments and four plagiogranites yield zircon U–Pb ages of 99.9, 98.4, 90.2 and 77.8 Ma, indicating that the sequence evolved over a considerable period of time. Most Sabzevar ophiolitic magmatic rocks are enriched in Large Ion Lithophile Elements (LILEs) and depleted in High Field Strength Elements (HFSEs), similar to SSZ-type magmatic rocks. They (except OIB-type lavas) have higher Th/Yb and plot far away from mantle array and are similar to arc-related rocks. Subordinate OIB-type lavas show Nb–Ta enrichment with high Light Rare Earth Elements (LREE)/Heavy Rare Earth Elements (HREE) ratio, suggesting a plume or subcontinental lithosphere signature in their source. The ophiolitic rocks have positive εNd (t) values (+5.4 to +8.3) and most have high $^{207}Pb/^{204}Pb$, indicating a significant contribution of subducted sediments to their mantle source. The geochemical and Sr–Nd–Pb isotope characteristics suggest that the Sabzevar magmatic rocks originated from a Mid-Ocean Ridge Basalt (MORB)-type mantle source metasomatized by fluids or melts from subducted sediments, implying an SSZ environment. We suggest that the Sabzevar ophiolites formed in an embryonic oceanic arc basin between the Lut Block to the south and east and the Binalud mountains (Turan block) to the north, and that this small oceanic arc basin existed from at least mid-Cretaceous times. Intraoceanic subduction began before the Albian (100–113 Ma) and was responsible for generating Sabzevar SSZ-related magmas, ultimately forming a magmatic arc between the Sabzevar ophiolites to the north and the Cheshmeshir and Torbat-e-Heydarieh ophiolites to the south-southeast.

1. Introduction

Ophiolites represent fragments of oceanic crust and upper mantle that were tectonically emplaced onto continents during orogenic events. They are generally exposed along suture zones, and play a key role in identifying ancient oceanic lithosphere and in paleogeographic reconstructions of orogenic belts (e.g., Coleman, 1977; Dilek, 2003; Dilek and Furnes, 2011). Ophiolites are particularly important for understanding the geologic evolution of Iran. The formation of modern Iran entailed closing first the Paleotethys and then the Neotethys oceans and accretion of Gondwana fragments (Cimmerian blocks) to the SW flank of Asia, a process which still continues today (Berberian and King, 1981; Knipper et al., 1986; Shafaii Moghadam and Stern, 2011; Shafaii Moghadam et al., 2013a). Iranian ophiolites demonstrate when and where ocean basins opened and closed and are widely distributed within Iran; the most well-known are the Paleotethys ophiolites in N and NE Iran and Neotethys ophiolites along the Bitlis–Zagros, Makran, Birjand–Nehbandan, Khoy–Maku and Sabzevar–Torbat-e-Heydarieh suture zones (Fig. 1).

The Sabzevar–Torbat-e-Heydarieh ophiolite belt (STOB) is situated in NE Iran (Fig. 1). It extends E-W for over 400 km and is bordered to the north by the major Sangbast–Shandiz strike–slip fault delimiting the Binalud Mountains (Kopet Dagh). To the south, this belt is bounded by the major Dorouneh sinistral strike–slip fault, separating it from the Lut Block (Nozaem et al., 2013). In this region, Neoproterozoic basement is also exposed (Fig. 2). The first detailed descriptions of these ophiolites were presented by Baroz et al. (1984) and post-ophiolitic Eocene

* Corresponding author.
E-mail addresses: hadishafaii@yahoo.com, hadishafaii@du.ac.ir (H.S. Moghadam).

http://dx.doi.org/10.1016/j.lithos.2014.10.004
0024-4937/

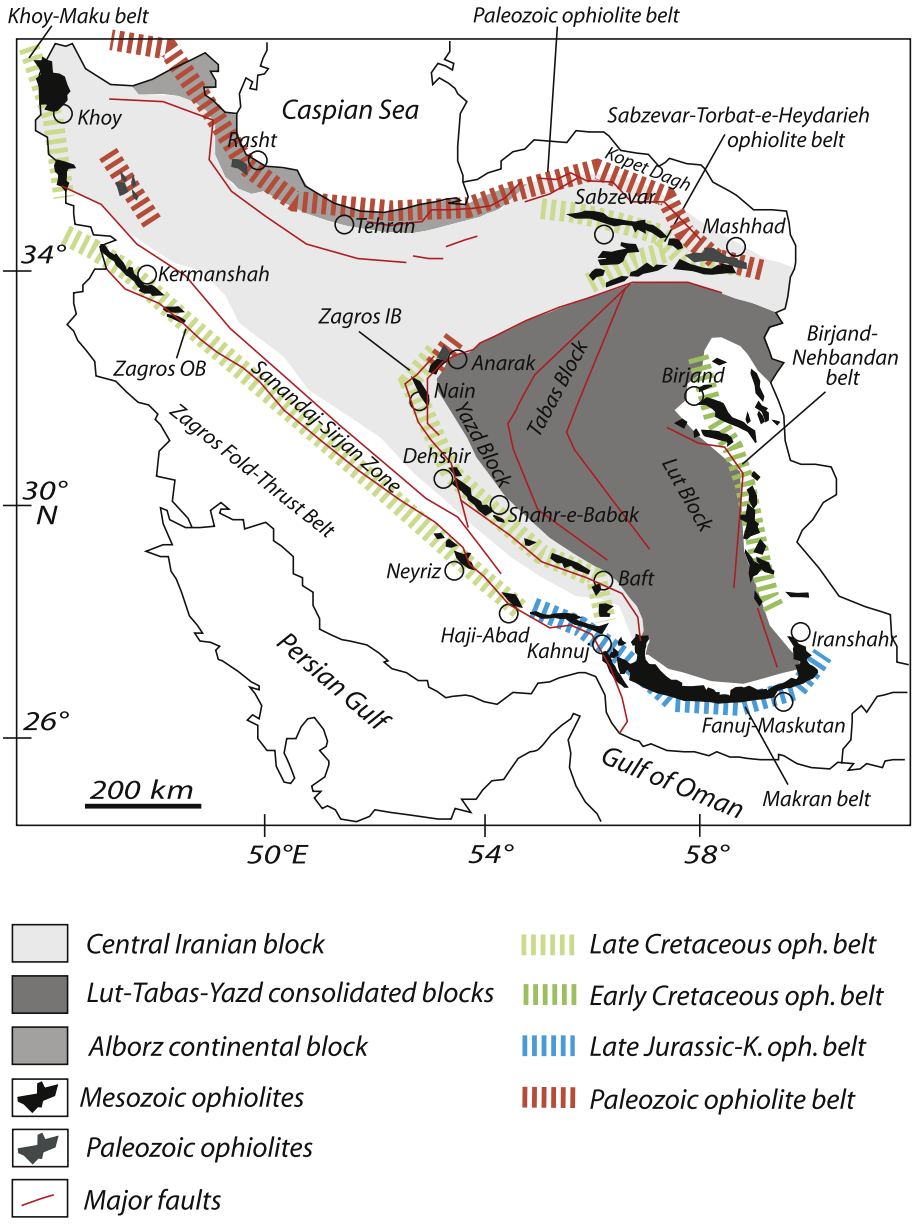

Fig. 1. Simplified geological map of Iran emphasizing the main ophiolitic belts (thick dashed lines) (colored on-line).

magmatic and younger rocks were studied by Lensch et al. (1980). The structure, petrography, and tectonic setting of the STOB were further studied by Ohnenestetter and Sider (1982), Baroz et al. (1983), Desmons and Beccaluva (1983), Shojaat et al. (2003) and Rossetti et al. (2010, 2013). The STOB contains ophiolitic remnants along four alignments (Fig. 2), separated by the Paleocene–Eocene Oryan sedimentary basin. These four alignments include: 1) ophiolites N and NW of Sabzevar town (Sabzevar and Forumad ophiolites); 2) ophiolites SSW of Sabzevar (Oryan–Bardaskan or southern Sabzevar ophiolites); 3) ophiolites north of Torbat-e-Heydarieh; and 4) thin ophiolitic slices SW of Neyshabour. These ophiolites are overlain by Upper Cretaceous to Paleocene extrusive rocks, volcanoclastic sediments, pelagic limestones and radiolarian cherts. To the NNE, the Sabzevar ophiolite is associated with an exhumed subduction zone with mafic protoliths metamorphosed to lawsonite-bearing blueschist (lawsonite, epidote, albite, crossite, phengite, garnet), granulite and greenschist (Omrani et al., 2013; Rossetti et al., 2010). The U–Pb age of these rocks is 106–107 Ma. The three ophiolitic alignments are separated by Paleocene–Eocene extensional basins filled with a transgressive series of flysch atop the ophiolite and spatially associated younger arc igneous rocks.

The ophiolites N of Sabzevar define a belt about 150 km long and 10–30 km wide. This ophiolite is part of the northern branch of the Neotethys Ocean (the Sabzevar Ocean) that opened and closed during the Late Cretaceous and may be related to the Lesser Caucasus ophiolites (Sengor, 1990). Berberian and King (1981) considered the Sabzevar ophiolites, like the Nain–Baft ophiolites, to be related to a seaway surrounding the Lut Block. Shojaat et al. (2003) suggested that the Sabzevar ophiolite was emplaced during NE-dipping subduction and Noghreyan (1982) proposed formation in a back-arc basin, based on the geochemistry of lavas and gabbros from the central Sabzevar chain (Baghjar region, Appendix 1). Shojaat et al. (2003) recognized three varieties of mafic rocks: 1) N-MORB type basalt and gabbro, 2) E-MORB type basalts and 3) basalts with arc signatures. Sabzevar ophiolitic volcano-sedimentary rocks were studied by Baroz and Macaudiere (1984). They distinguished four lithostratigraphic units, from Campanian in the lower parts to Paleocene in the upper parts, including alkaline to

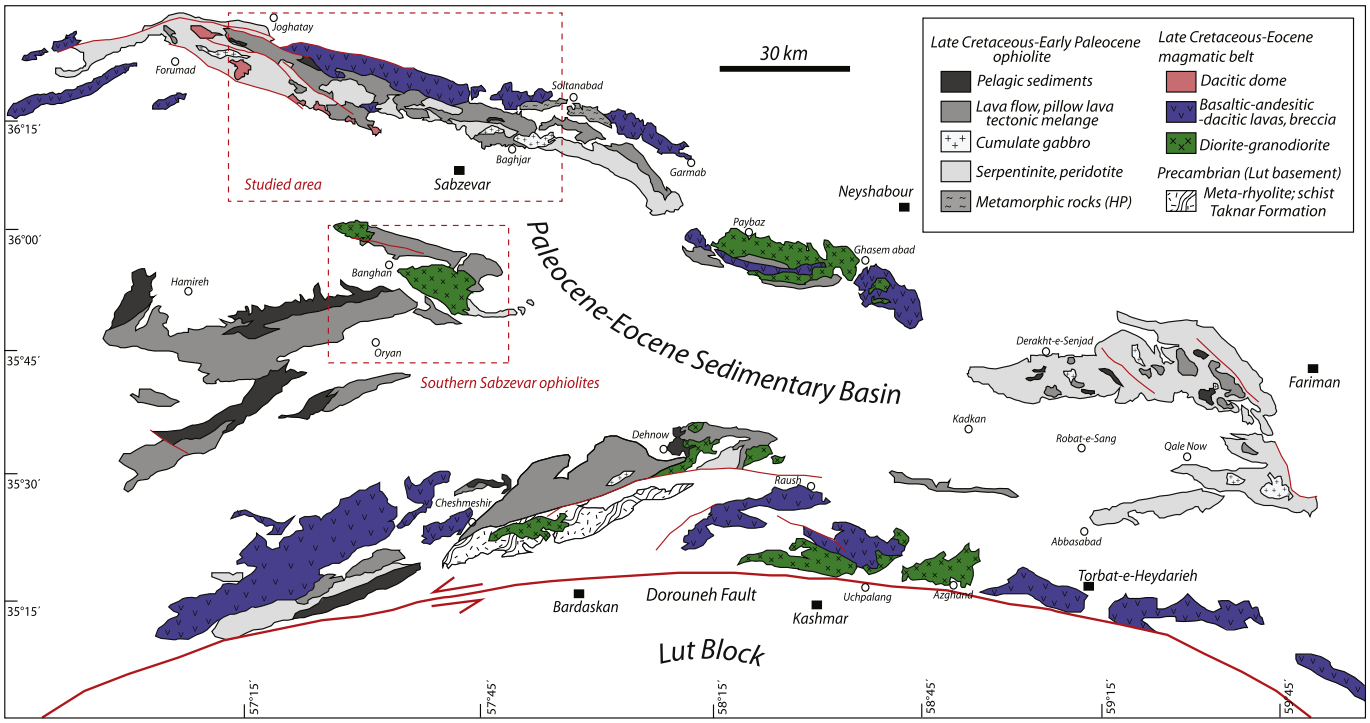

Fig. 2. Geological map of the Sabzevar–Torbat-e-Heydarieh region, north of the Dorouneh Fault, with emphasis on the distribution of ophiolitic and arc-related rocks (colored on-line).

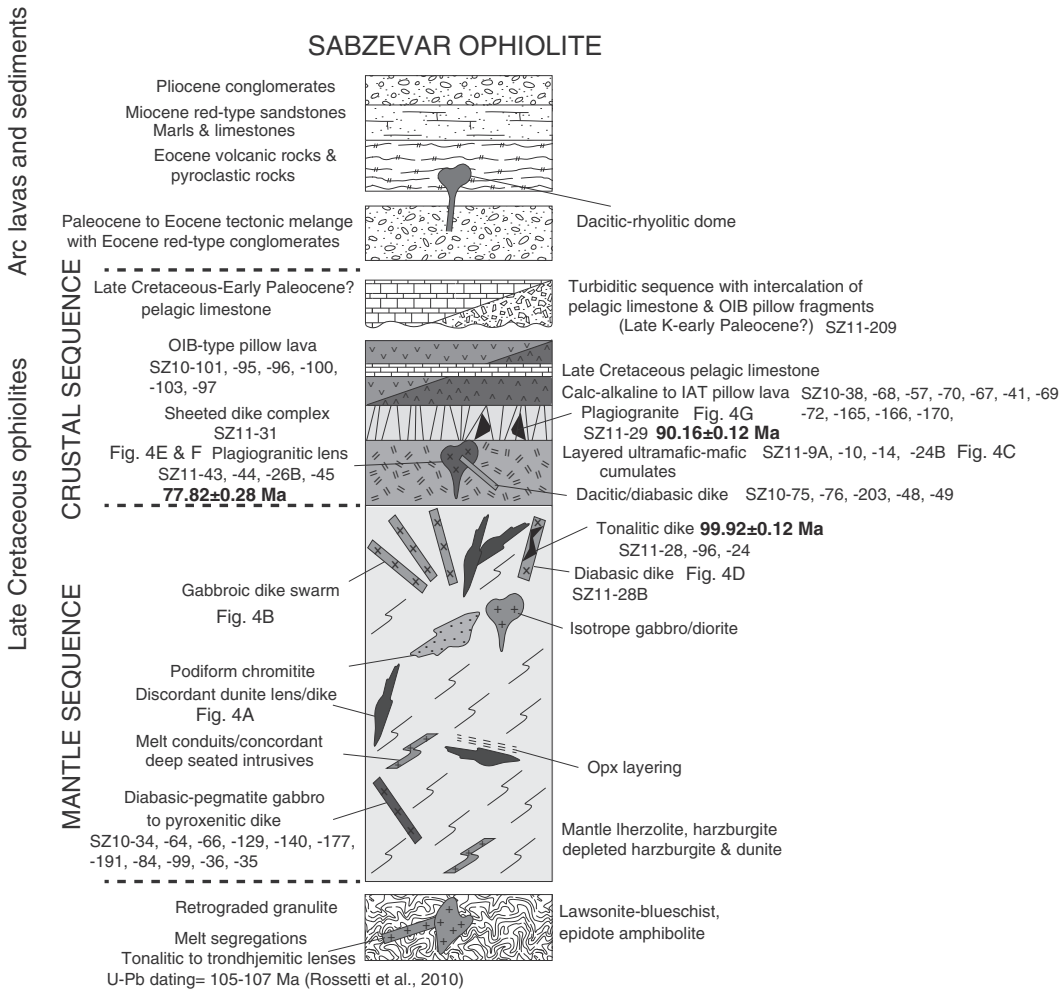

Fig. 3. Simplified stratigraphic columns displaying idealized internal lithologic successions in Sabzevar ophiolites.

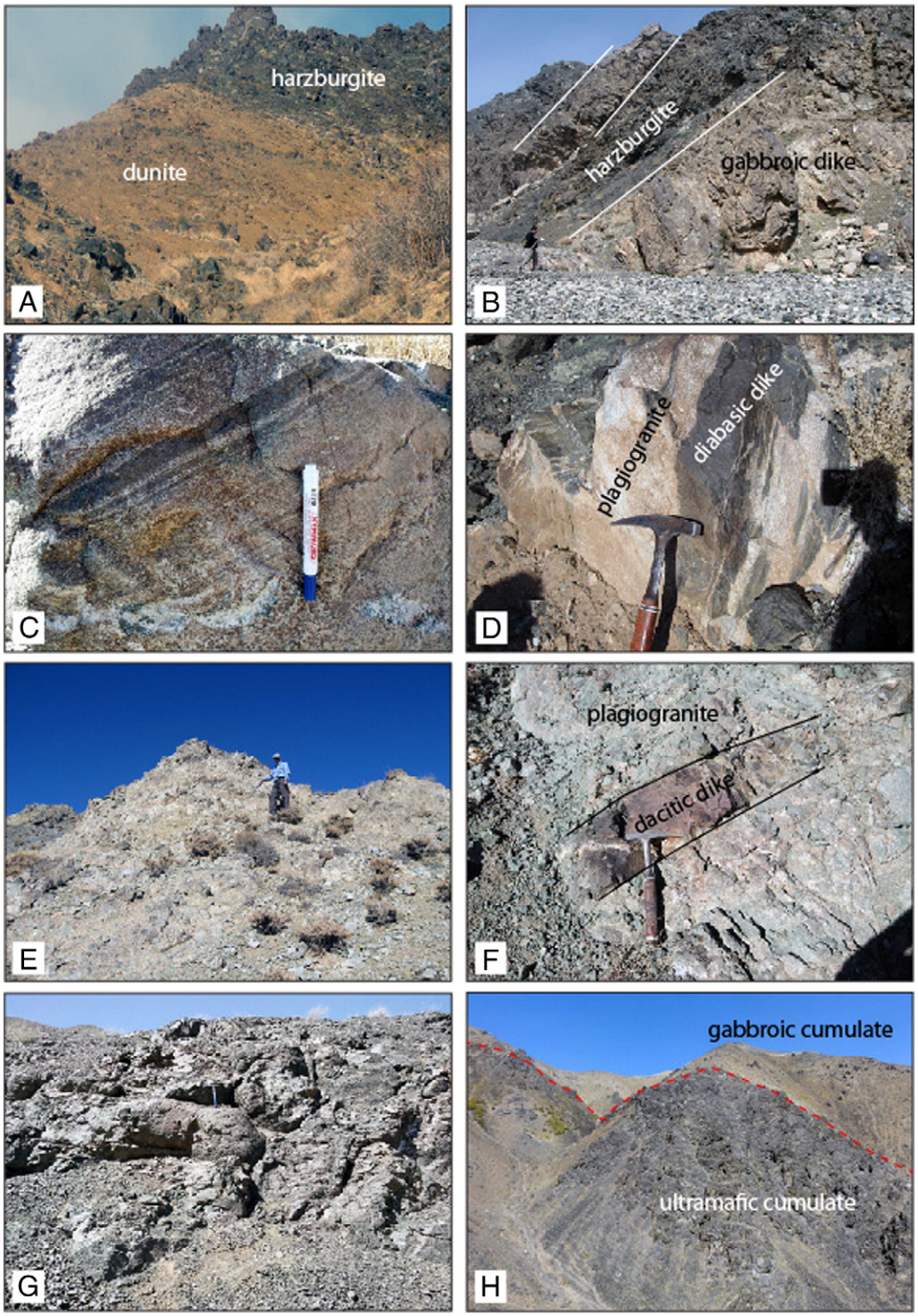

Fig. 4. Field photographs of Sabzevar ophiolites. A—sub-concordant dunites within mantle harzburgites in Kuh Siah region. B—thick (2–3 m) gabbroic dikes within mantle harzburgites in Shareh village. C—Soleimanieh layered ultramafic-mafic cumulates. D—plagiogranitic dikes injected into diabasic dikes of mantle sequence. E—plagiogranitic lenses injected into layered cumulate gabbros near Sang-e-Sefid village. F—injection of thin dacitic dikes within Sang-e-Sefid plagiogranites. G—outcrop of pillow lavas near Afchang. H—the concordant contact between cumulate ultramafic rocks and cumulates gabbros at southern Sabzevar ophiolites (colored on-line).

calc-alkaline pillow lavas, litharenites, breccias and agglomerates with pelagic sediments. Their geodynamic reconstruction included: 1) generation of oceanic crust in a back-arc basin in Middle to Late Cretaceous times; 2) deposition of the volcano-sedimentary series, fed from a Late Cretaceous–Paleocene arc; and 3) collision of the arc with the Lut Block. Rossetti et al. (2010) argued that the Sabzevar granulites formed during subduction of a branch of Late Jurassic–Early Cretaceous back-arc oceanic system (part of the Sistan Ocean, as suggested by Barrier and Vrielynck, 2007), with northward subduction polarity (toward Eurasia).

In this paper, new TIMS U–Pb zircon as well as biostratigraphic ages, whole-rock geochemistry and Sr–Nd–Pb isotopic data of Sabzevar magmatic rocks are presented and used to discuss the geodynamic evolution of the Sabzevar suture zone. These data are integrated to discuss the time, type and processes of crustal accretion within the Sabzevar oceanic basin. Our discussion includes a synthesis of the development

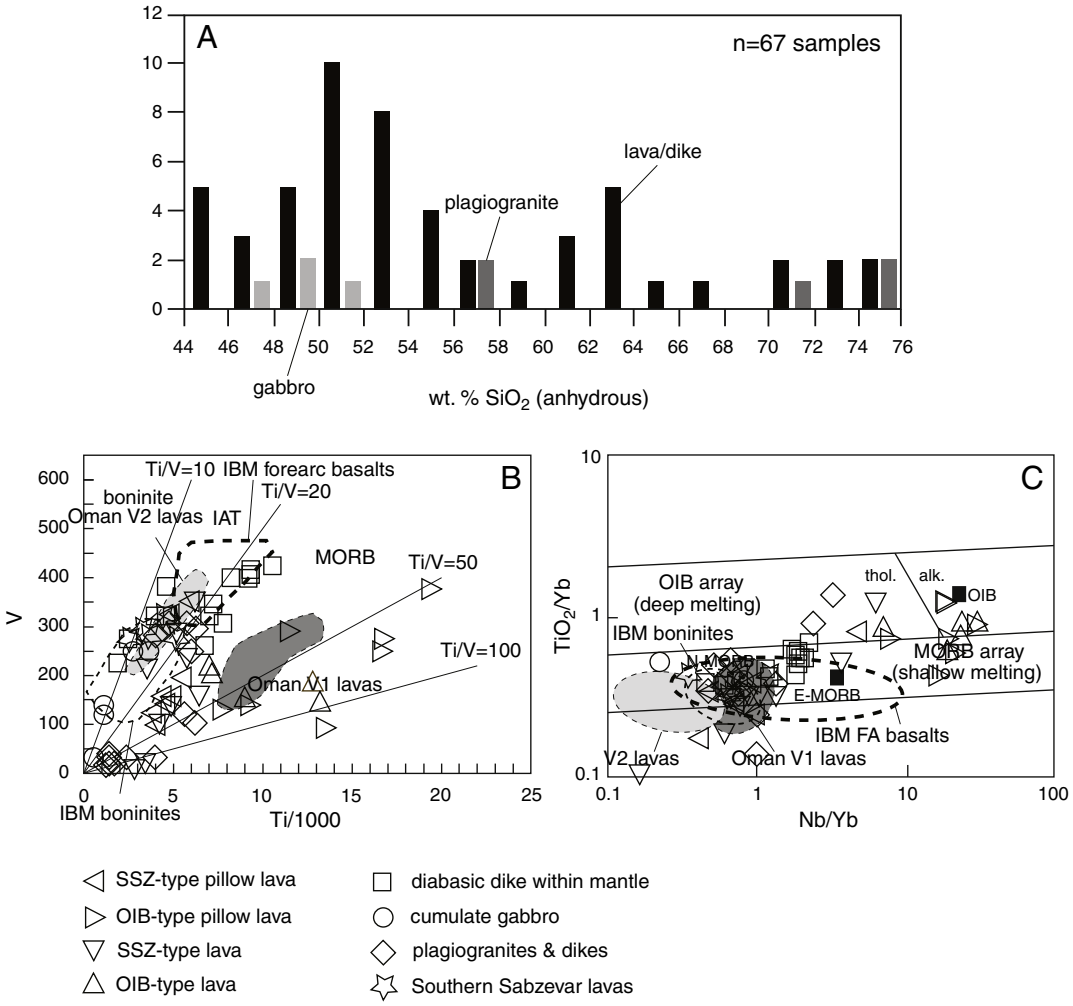

Fig. 5. (A) Histograms of wt.% SiO_2 (recalculated to 100% anhydrous) demonstrating a trimodal composition of the Sabzevar magmatic rocks. Ti vs. V (B) and TiO_2/Yb vs. Nb/Yb (C) compositional variations of Sabzevar ophiolitic magmatic rocks. TiO_2/Yb vs. Nb/Yb diagram modified after Pearce (2008) and Ti vs. V diagram modified after Shervais (1982). Data for Oman ophiolites are from Godard et al. (2003) and for Izu–Bonin–Mariana (IBM) forearc from Reagan et al. (2010).

of the ophiolite NNW of the Sabzevar town (Sabzevar ophiolite) and comparison with ophiolites SSW of Sabzevar (the Oryan–Bardaskan ophiolites). Detailed field, age and geochemical data on the Forumad and Torbat-e-Heydarieh ophiolites will be presented elsewhere.

2. Field occurrence

Harzburgite, lherzolite, dunite and chromitite are the major components of the Sabzevar mantle sequence (Fig. 4A). Harzburgites are crosscut by diabasic, gabbroic, gabbro-pegmatitic, wehrlitic and pyroxenitic dikes (Fig. 3). Gabbroic dike swarms, averaging 3–5 m thick, injected into mantle harzburgite with discordant dunite lenses, are common near Shareh village (Fig. 4B; Appendix 2). Lherzolites in most cases are late magmatic, produced during migration and percolation of MORB- and/or SSZ-type basaltic melts through depleted mantle harzburgites with crystallization of clinopyroxenes (with or without plagioclase) and Al-rich spinel (Shafaii Moghadam et al., 2013c). Most peridotites are foliated, with foliation marked by oriented orthopyroxene (and/or spinel) and rarely clinopyroxene (secondary foliation, S_2) porphyroclasts. Dunites occur as discordant lenses and dikes within orthopyroxene-rich harzburgites (Fig. 3). Podiform and nodular-type chromitites with thin dunitic haloes are locally present. Pegmatite clinopyroxenitic and gabbroic dikes crosscut both depleted harzburgites/dunites and chromitites. Large chromitite deposits occur in the Gaft and Forumad regions with both high Cr# and low Cr# chromites, denoting crystallization of chromites from early MORB-type and then boninitic-type melts (Shafaii Moghadam et al., 2013c). Depleted SSZ-type wehrlitic (rarely gabbroic) sills and dikes crosscut all units including chromitite, dunite and harzburgite (Shafaii Moghadam et al., 2013c). The occurrence of depleted harzburgite, dunite, wehrlitic dikes/sills and chromitite marks a Moho Transition Zone in the region.

The Sabzevar gabbroic rocks are divided into 1) isotropic to pegmatitic gabbroic lenses within mantle harzburgites and 2) crustal cumulate gabbro/gabbronorite/leucogabbro (with minor diorite) with local layering associated with minor ultramafic cumulates in Soleimanieh, Sang-e-Sefid and Baghjar regions (Fig. 4C; Appendix 1). Basaltic to dacitic and microdioritic dikes crosscut cumulate gabbros. Brown-amphibole (magmatic) rich cumulate rocks are common near the Qare-Qoli village, crosscutting the early dry pyroxenitic–wehrlitic–gabbroic cumulates. Similar highly hydrous cumulates are common in the root of volcanic arcs and represent “amphibole sponges” of arc crust (e.g., Davidson et al., 2007; Larocque and Canil, 2010 and references therein). A highly fragmented and sheared sheeted dike complex, but clearly with dike-into-dike relationships, with early basaltic to andesitic basaltic dikes and late dacitic dikes, is present near Baghjar (Appendix 1). Plagiogranite occurs as 1) lenses within cumulate and coarse-grained gabbro associated with abundant crosscutting micro-dioritic to dacitic (and even basaltic) dikes (Fig. 4E and F); 2) as veins/dikes, crosscutting diabasic dikes within

mantle harzburgites (Fig. 4D); and 3) as small pockets within the sheeted dike complex. They are rarely injected into basaltic to andesitic lavas.

Pillowed and massive basalts are common in the Sabzevar crustal sequence (Fig. 4G). They are found near the Afchang, Belash–Abad, Dorofk and Aliak villages (Appendix 1). Pelagic sediments stratigraphically cover the pillow lava sequence and/or are interbedded with them. Andesitic dikes (1–1.5 m in thickness) occasionally crosscut the pillow lavas. These pillow lavas are both OIB- and SSZ-types (see next sections). These two types of pillow lavas are geographically distributed without clear relationships, but both of them are overlain and/or intercalated with Late Cretaceous pink limestones. The lavas grade upwards into turbiditic sandstone/breccias and pyroclastic deposits containing OIB-type basaltic (pillow-like) fragments. Late Cretaceous to early Paleocene pelagic limestone is interlayered with these turbidites. Metamorphic rocks including blueschists, micaschists and retrogressed mafic

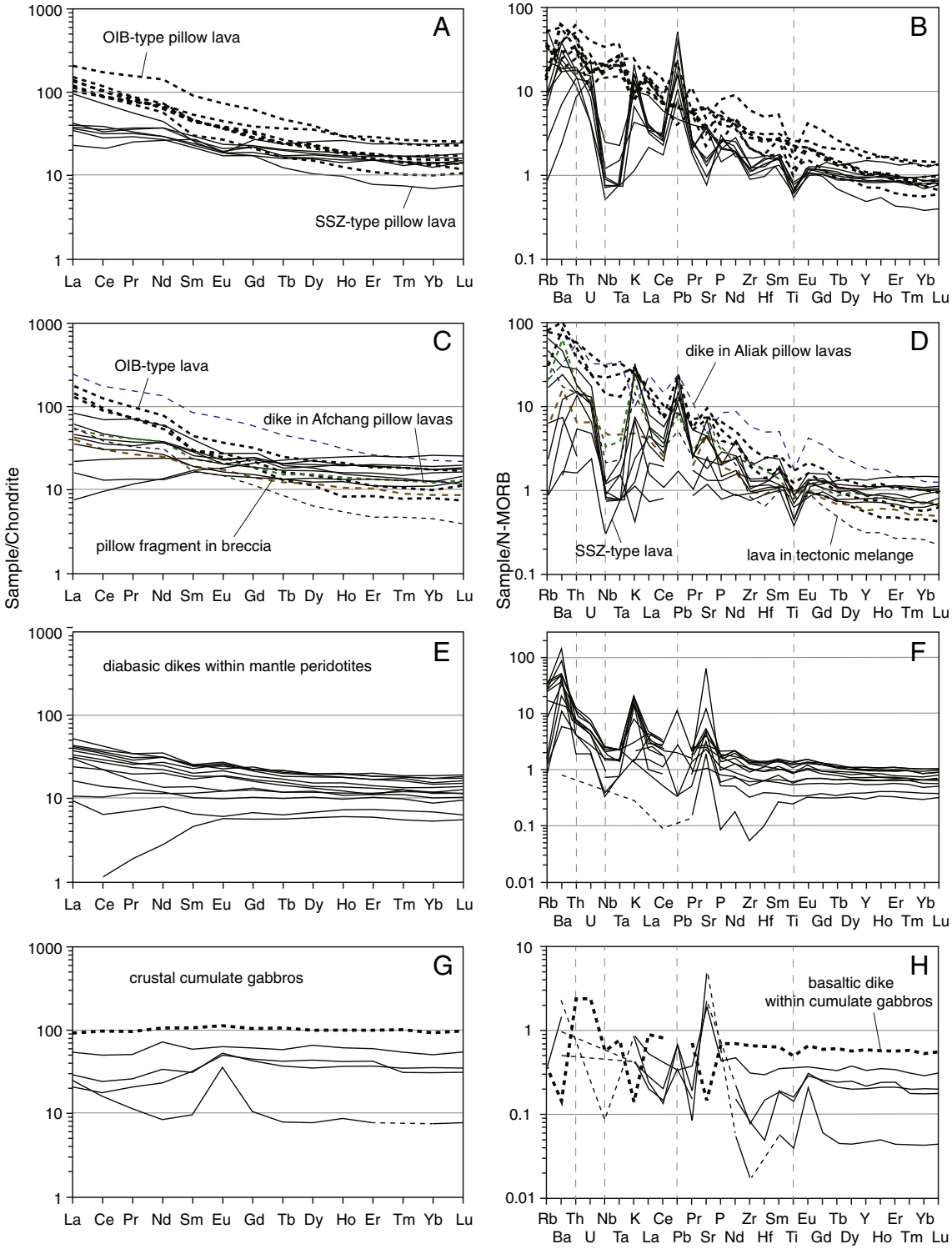

Fig. 6. Chondrite-normalized REE patterns (chondrite abundances from McDonough and Sun, 1995) and N-MORB normalized multi-element patterns (N-MORB concentrations from Sun and McDonough, 1989) for Sabzevar magmatic rocks.

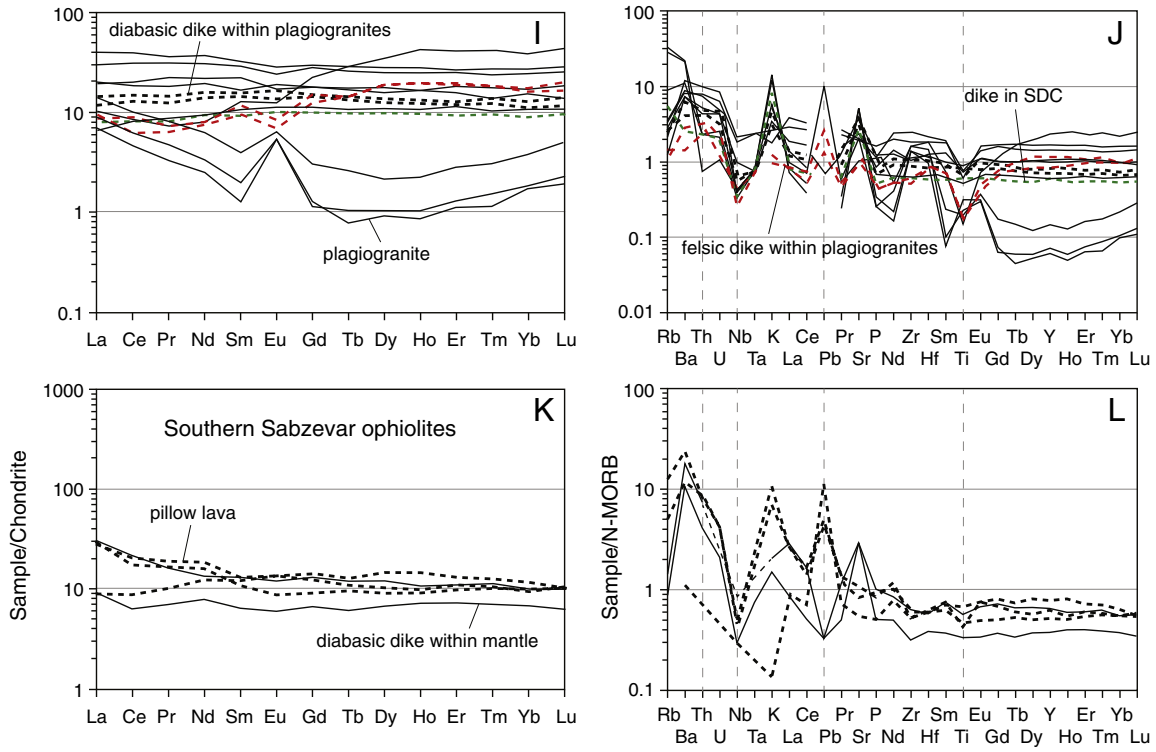

Fig. 6 (*continued*).

granulites with leucocratic segregations (ca. 106–107 Ma) are found near Soltan–Abad and WNW of Delbar villages (Appendices 1 and 2) and are considered to have formed in a hot subduction setting (Rossetti et al., 2010).

The Sabzevar ophiolite is associated with a tectonic mélange containing ophiolitic and Paleocene to Eocene arc-related lavas, probably formed via tectonic movements during Late Eocene time, likely the age of Sabzevar ophiolite emplacement. Red Eocene polygenic conglomerates seal the ophiolite contacts. Eocene calc-alkaline basaltic, andesitic to dacitic rocks and pyroclastic rocks (agglomerates, tuffs and lapilli tuffs) intrude and cover the ophiolites, mainly north of the Sabzevar ophiolites.

The ophiolites SSW of Sabzevar (Oryan–Bardaskan ophiolites) include mantle harzburgites with crosscutting diabasic and microgabbroic dikes. Crustal cumulate gabbros–gabbronorites are found near Torosk village. Aphyric to rarely porphyritic andesitic dikes (~0.5–1 m thick) crosscut the cumulate gabbros and gabbronorites. These gabbros are underlain by ultramafic cumulates including cumulate harzburgites and dunites (Fig. 4H). Impregnated dunites (with clinopyroxene) are common. This ultramafic sequence is crosscut by gabbroic to dioritic dikes. Pillow lavas with intercalation of pelagic limestones are common near Garzak village.

3. Petrography

Mantle harzburgites are variably serpentinized and relicts consist of olivine, large orthopyroxene porphyroclasts, and spinel with minor (<3%) clinopyroxene. Olivine is anhedral and often shows typical kink-band deformation. Orthopyroxene occurs as subhedral to generally tabular grains. Dunites are strongly serpentinized and only a few relicts of olivine and spinel survive. Lherzolites are most common south of Afchang (Appendix 1) and near the Shareh villages (shown in Appendix 2) and have gradational contacts with harzburgites. Most lherzolites show melt-pocket shaped domains, consisting chiefly of large clinopyroxene, olivine and vermicular, light brown (Al-rich) spinels (Shafaii Moghadam et al., 2013c). These pockets are generally characterized by coarse-grained crystals forming an equigranular texture. Lherzolites have anhedral olivine, large orthopyroxene porphyroclasts (~5–6 mm, up to 10 mm), and smaller clinopyroxene grains. Vermicular light brown spinels are common. Plagioclase-bearing lherzolites are characterized by the presence of small, anhedral blebs of plagioclase (usually highly saussuritized) interstitial between olivine and orthopyroxene, surrounding the large spinel grains and/or crosscutting clinopyroxene or spinel grains (Shafaii Moghadam et al., 2013c).

Gabbroic dikes within mantle rocks contain clinopyroxene and highly altered plagioclase. Clinopyroxenitic dikes contain large (4–5 mm) clinopyroxene grains with rare serpentinized olivines (5–6 vol.%). Diabasic dikes within the mantle sequence include traces of clinopyroxene, green amphibole and altered plagioclase with minor oxides. Crustal dry gabbros and gabbronorites show orthocumulate textures with clinopyroxene, orthopyroxene and interstitial plagioclase. Plagioclase is a late-stage phase and occupies the space between cumulus pyroxenes. Olivine is rare in gabbros but common in olivine gabbros. Clinopyroxene, but mostly plagioclase shows resorbed margins with overgrowth of second-generation clinopyroxene and plagioclase, respectively. Hydrous gabbros contain brown to green amphiboles interstitial between other minerals. Pillow to massive lavas have mostly andesitic to dacitic composition and are rarely basaltic. These lavas are porphyritic with microlitic groundmass. Andesitic lavas have plagioclase phenocrysts (1-3 mm av.) and microlites (~0.1–0.3 mm). Clinopyroxene has variable size (0.2–2 mm) and is absent in dacitic lavas, whereas quartz and oxides (ilmenite/magnetite) are common. Small crystals (0.2–0.3 mm) of brown amphibole are common in OIB-type pillow lavas. The lavas were metamorphosed in the greenschist facies with the formation of actinolite, albite, prehnite, chlorite, epidote, titanite and palagonite. Plagiogranites are compositionally trondhjemitic and/or tonalitic and contain plagioclase laths, quartz, actinolite and oxides. Dikes in crustal gabbros, plagiogranites, pillow lavas and within sheeted dike complexes are aphyric to poorly phyric, with basaltic, andesitic and even dacitic compositions. Basaltic dikes have clinopyroxene and plagioclase

Table 1
Sr–Nd–Pb isotope composition of the Sabzevar ophiolitic rocks.

Sample	Rock type	Rb	Sr	$^{87}Sr/^{86}Sr$	1SE	$^{87}Rb/^{86}Sr$	$(^{87}Sr/^{86}Sr)i$	Sm	Nd	$^{143}Nd/^{144}Nd$	1SE	$^{147}Sm/^{144}Nd$
SZ10-36	Lava flow	1.00	119.80	0.7045	0.000013	0.0241	0.7045	3.9180	14.7400	0.5129	0.000009	0.1600
SZ10-69	Pillow lava	5.00	106.70	0.7045	0.000006	0.1355	0.7043	4.3940	16.1700	0.5129	0.000004	0.1636
SZ11-28A	Plagiogranite	17.20	459.00	0.7040	0.000003	0.1084	0.7038	0.3100	1.6000	0.5130	0.000020	0.1167
SZ11-28B	Diabasic dike	19.20	426.00	0.7040	0.000002	0.1304	0.7038	1.7500	5.3000	0.5131	0.000005	0.1988
SZ11-29	Plagiogranite (SDC)	1.70	244.00	0.7055	0.000003	0.0202	0.7055	1.6700	4.5000	0.5130	0.000007	0.2234
SZ11-31	Dike in SDC	3.10	230.00	0.7057	0.000004	0.0390	0.7057	1.4800	4.5000	0.5130	0.000007	0.1980
SZ11-35	Diabasic dike (Hz)	4.70	225.00	0.7038	0.000003	0.0604	0.7037	3.8500	14.4000	0.5130	0.000006	0.1610
SZ11-44	Plagiogranite (gab)	1.80	202.00	0.7043	0.000014	0.0258	0.7043	4.5400	14.7000	0.5130	0.000005	0.1859
SZ11-49	Microdioritic dike	1.50	252.00	0.7053	0.000010	0.0172	0.7052	2.2600	6.7000	0.5130	0.000013	0.2031
SZ11-51	Dacitic lava	0.20	112.00	0.7052	0.000018	0.0052	0.7052	3.5300	11.1000	0.5131	0.000010	0.1915
SZ11-74	Gabbronorite	0.39	133.60	0.7041	0.000004	0.0085	0.7041	0.6632	1.5100	0.5130	0.000009	0.2644
SZ11-91	Lava flow	0.50	104.50	0.7056	0.000006	0.0138	0.7056	2.6100	6.4000	0.5130	0.000009	0.2455

microphenocrysts with palagonitized glass, while felsic dikes have plagioclase microphenocrysts with crypto-felsic groundmass.

4. Whole rock geochemistry

We selected sixty-seven relatively fresh samples from the Sabzevar ophiolites for whole rock analysis, including pillowed and massive lavas, dikes in pillow sequences, pillow fragments in Late Cretaceous–Early Eocene turbidites, cumulate gabbros and their associated dikes, plagiogranites, intermediate to felsic dikes crosscutting the plagiogranites and diabasic dikes within mantle peridotites. Analytical methods for whole rock major, trace, REE, mineral composition and Sr–Nd–Pb isotopic analyses as well as U–Pb zircon dating are presented in the Supplementary Data. Bulk rock major and trace element data are available in Supplementary Table 1. Sabzevar magmatic rocks are mostly altered, characterized by a wide range of LOI (0.4 to 14.3 wt.%). This alteration could affect the mobile elements such as Sr, Rb, Ba, K, and $^{87}Sr/^{86}Sr$. However the abundances of incompatible elements (e.g., REE, Th, U, Nb, Ta, Zr, Hf, Ti and Pb) and Nd–Pb isotopic compositions are minimally affected by moderate alteration (e.g., Celik et al., 2013; Chiaradia, 2009).

Our geochemical dataset (as well as field and petrographic data) shows that the Sabzevar ophiolites include very large proportions of intermediate to acidic magmatic rocks. The SiO_2 histogram (recalculated as volatile free, 100%) (Fig. 5A) shows a trimodal distribution where mafic igneous rocks are dominant but intermediate and acidic magmatic rocks are also common.

4.1. Pillow lavas

Eighteen pillow basalt samples were analyzed in this study. Two types of pillow lavas have been recognized: 1) OIB-type (7 samples) and 2) SSZ-type (11 samples). OIB-type pillow lavas are found near the Afchang and Aliak villages (Appendix 1) and contain low concentrations of SiO_2, high TiO_2 and variable Mg# ($100Mg/Mg + Fe^t$) (Supplementary Table 1). SSZ-type pillow lavas are mafic to felsic with variable SiO_2 and Mg# and low TiO_2. In a Ti vs. V diagram (Shervais, 1982), OIB-type pillow lavas tend to plot in the OIB field whereas the SSZ-type pillow lavas plot in the island-arc tholeiitic (IAT) field (Fig. 5B). In a TiO_2/Yb vs. Nb/Yb diagram (Pearce, 2008), the OIB-type pillow lavas have higher TiO_2/Yb and Nb/Yb ratios and plot near the MORB to OIB arrays (shallow to deep melting) whereas SSZ-type pillow lavas plot near the MORB and Oman V1 lavas (Fig. 5C).

The OIB-type lavas have fractionated REE patterns with strong light REE (LREE) enrichment ($La_{(n)}/Yb_{(n)} = 3.9–14.1$). They are characterized by positive anomalies in Rb, Ba, Th, U and K ($Th_{(n)}/La_{(n)} = 2.5–3.7$) relative to N-MORB but do not show negative anomalies in Nb–Ta ($Nb_{(n)}/La_{(n)} = 1.4–1.7$) (Fig. 6A and B). The SSZ-type lavas are similarly enriched in LREE relative to heavy REEs (HREE) ($La_{(n)}/Yb_{(n)} = 0.98–13.7$) and enriched in Ba, Th, U, K and Pb relative to N-MORB but show strong Nb–Ta–Ti negative anomalies with respect to the LREE ($Nb_{(n)}/La_{(n)} = 0.16–0.34$) (Fig. 6A and B). These characteristics are similar to arc basalts from SSZ environments (e.g, Pearce, 2014). Basaltic dikes crosscutting both OIB-type and SSZ-type pillow lavas have OIB and calc-alkaline signatures, respectively (Fig. 6C and D).

4.2. Massive lavas

Twelve massive basalt samples were analyzed. Massive lavas in the Sabzevar ophiolites can also be subdivided into OIB and SSZ-types. OIB-type lavas (3 samples) are mafic with SiO_2 and Mg# ranging 40.7–51.2 wt.% and 35.1–48.3, respectively. Their TiO_2 content is surprisingly high (Supplementary Table 1). SSZ-type lavas have variable contents of SiO_2 but low TiO_2 contents. In the Ti vs. V diagram most SSZ-type lavas plot in the IAT field and/or have low Ti and V content similar to calc-alkaline lavas. OIB-type massive lavas have lower TiO_2 contents than OIB-type pillow lavas and plot near the Oman V1 (MORB-like) lavas. In the TiO_2/Yb vs. Nb/Yb diagram (Pearce, 2008), the OIB-type lavas plot near the MORB to OIB arrays (shallow to deep melting) whereas SSZ-type lavas plot near the MORB and Oman V1 lavas (Fig. 5C).

OIB-like massive lavas are characterized by enrichment in LREEs relative to HREEs and Rb, Ba, Th, U, and Nb–Ta enrichments relative to N-MORB. A pillow fragment within Late Cretaceous–Early Paleocene turbidites (SZ11-209) also has an LREE-enriched pattern that lacks Nb–Ta negative anomalies similar to OIB-type lavas. In contrast, SSZ-type lavas have LREE depleted to fractionated REE patterns ($La_{(n)}/Yb_{(n)}$ ~ 0.3–6.5) with negative Nb–Ta–Ti anomalies with respect to the LREE ($Nb_{(n)}/La_{(n)} = 0.2–0.6$) and Ba, U, Pb, and Th positive anomalies, similar to IAT and calc-alkaline lavas, respectively. The lavas within the tectonic mélange (Appendix 1) also have calc-alkaline signatures.

4.3. Diabase dikes within mantle peridotites

Thirteen diabase dike samples were analyzed. Most of the diabasic dikes within mantle peridotites are mafic to slightly intermediate with Mg# ranging between 37.9 and 75.9 (Supplementary Table 1). Their TiO_2 contents are mostly higher than in SSZ-type lavas. In a Ti vs. V diagram (Shervais, 1982) these dikes plot in boninite-IAT to MORB and/or IBM forearc basalt domains (Fig. 5B). Most dikes have higher TiO_2/Yb and Nb/Yb and follow the MORB array (Pearce, 2008) (Fig. 5C). Dikes are characterized by depleted to flat and LREE-enriched patterns ($La_{(n)}/Yb_{(n)} = 0.9–3.3$), but all show Nb–Ta negative anomalies and Ba, U, Sr, and Th enrichment, resembling both SSZ lavas (Fig. 6E and F).

($^{143}Nd/^{144}Nd$)i	U	Th	206/204	207/204	208/204	206/204i	207/204i	208/204i	eNd(100)
0.5128	0.41	1.70	18.448	15.572	38.491	17.996	15.550	37.876	5.40
0.5128	0.57	1.90	18.458	15.584	38.489	17.514	15.538	37.458	5.59
0.5129	0.10	0.25	18.251	15.567	38.265	18.231	15.566	38.248	7.92
0.5129	0.09	0.23	18.307	15.601	38.384	18.289	15.601	38.369	8.31
0.5129	0.08	0.23	18.426	15.646	38.527	18.410	15.645	38.512	7.27
0.5129	0.10	0.28	18.107	15.600	38.053	18.088	15.600	38.035	7.60
0.5129	0.31	1.29	18.417	15.500	38.422	18.355	15.497	38.338	7.54
0.5129	0.30	0.92	18.663	15.573	38.696	18.603	15.570	38.636	7.52
0.5128	0.15	0.49	18.736	15.573	38.717	18.706	15.572	38.685	6.12
0.5129	0.22	0.64	18.396	15.544	38.325	18.352	15.542	38.283	8.32
0.5129	0.01	0.02	18.348	15.598	38.377	18.316	15.597	38.338	7.16
0.5129	0.11	0.19	18.358	15.573	38.386	18.336	15.572	38.373	6.98

4.4. Cumulate gabbros

Four cumulate gabbro samples were analyzed. Cumulate gabbros have variable SiO_2, Al_2O_3, CaO, TiO_2 and Mg# (Supplementary Table 1). Variable contents of CaO, MgO and Al_2O_3 are related to different accumulations of clinopyroxene and plagioclase in these rocks. These rocks have flat to LREE-depleted REE patterns ($La_{(n)}/Yb_{(n)}$ = 0.7–1.1) except sample SZ11-10 with a convex-upward pattern and enrichment in Eu due to plagioclase accumulation (Fig. 6G). These characteristics are associated with negative Nb–Ta anomalies with respect to the LREE (Fig. 6H) and so display an SSZ environment for formation of these rocks.

4.5. Plagiogranites and associated dikes

Eight plagiogranite samples were analyzed. Plagiogranites contain high and variable SiO_2 and moderate TiO_2 contents (Supplementary Table 1). Felsic dikes crosscutting the plagiogranites have 70.6–73.1 wt.% SiO_2 and 0.22–0.23 wt.% TiO_2 while diabase dikes within plagiogranites contain less SiO_2 (58.1–58.2 wt.%) but have higher TiO_2 (0.97–1.04 wt.%) contents. Plagiogranites show three different REE patterns (Fig. 6I and J): 1—LREE depleted ($La_{(n)}/Yb_{(n)}$ = 0.3) and associated with negative Nb–Ta ($Nb_{(n)}/La_{(n)}$ = 0.4) and positive Ba, U, K, and Th anomalies relative to N-MORB. 2—Approximately flat ($La_{(n)}/Yb_{(n)}$ = 0.6–1.5), associated with negative Nb–Ta anomalies ($Nb_{(n)}/La_{(n)}$ = 0.5–0.6) and enrichment in large ion lithophile elements (LILEs) relative to N-MORB. The first two groups' patterns resemble those of island-arc tholeiites. 3—Spoon-like pattern with LREE enrichment ($La_{(n)}/Yb_{(n)}$ = 3.7–5.2); these also show negative Nb–Ta ($Nb_{(n)}/La_{(n)}$ = 0.3–0.6) and positive Th anomalies relative to N-MORB, similar to highly depleted tholeiites or boninites. Diabase dikes (in plagiogranites) and one dike within SDC have flat REE patterns ($La_{(n)}/Yb_{(n)}$ = 0.9–1.1) while felsic dikes have depleted LREE patterns ($La_{(n)}/Yb_{(n)}$ = 0.5). These dikes show negative Nb–Ta ($Nb_{(n)}/La_{(n)}$ =0.3–0.6) and positive Th anomalies relative to N-MORB. The geochemical features of all three groups are similar to those of magmas generated at convergent margins (Pearce, 2008).

4.6. Lavas from southern Sabzevar ophiolites

For comparison, we analyzed three pillow lavas and two diabase dikes injected within harzburgites from southern Sabzevar ophiolites. The southern ophiolites have not been studied before. Southern Sabzevar ophiolitic magmatic rocks have mafic to intermediate compositions. The rocks have low TiO_2 and plot in the IAT field on the V vs. Ti diagram of Shervais (1982) (Fig. 5B). The rocks have low TiO_2/Yb and Nb/Yb and are similar to Izu–Bonin–Mariana (IBM) forearc basalts (Fig. 5C). These rocks show both LREE-enriched ($La_{(n)}/Yb_{(n)}$ = 2.8–3.1) and flat REE patterns ($La_{(n)}/Yb_{(n)}$ = 0.8–1.4). These rocks show negative Nb–Ta ($Nb_{(n)}/La_{(n)}$ = 0.2–0.3) and positive Th anomalies relative to N-MORB (Fig. 6K and L).

5. Sr–Nd–Pb isotopes

Initial $^{87}Sr/^{86}Sr$ calculated at 100 Ma (the most common U–Pb zircon crystallization age of Sabzevar ophiolite) ranges from 0.7037 to 0.7057 (Table 1), higher than for oceanic tholeiites. This may reflect exchange between rock and seawater during alteration (Kawahata et al., 2001; McCulloch et al., 1981). Dacitic lava flow (SZ11-51) and a diabasic dike within mantle harzburgite (SZ11-28B) are more radiogenic compared to other samples whereas other felsic lava (SZ10-39) and Dorofk pillow lava (SZ10-69) are less radiogenic. Initial εNd (t, CHUR) calculated at 100 Ma ranges from +5.4 to +8.3 for Sabzevar magmatic rocks (Table 1). Lower $^{143}Nd/^{144}Nd$ for two calc-alkaline lavas (SZ10-36 and SZ10-69) may indicate a greater contribution of subducted sediments in the source area. Sabzevar magmatic rocks have Nd isotopic compositions that mostly overlap with those of the least radiogenic MORB and with Oman and Neyriz ophiolitic rocks (Fig. 7A). All the Sabzevar rocks have less radiogenic Nd compared to IBM forearc basalts (Fig. 7A), which may reflect an Indian mantle domain.

The initial $^{206}Pb/^{204}Pb$ and $^{208}Pb/^{204}Pb$ values are quite variable, between 17.51 and 18.71 and between 37.46 and 38.68, respectively (Table 1). The Dorofk pillow lava (SZ10-69) has the least radiogenic Pb. Most samples have high $^{207}Pb/^{204}Pb$ relative to the Northern Hemisphere Reference Line (Hart, 1984) (Fig. 7B), ranging from 15.50 to 15.65, indicating higher contribution of subducted sediments to their mantle source relative to Oman and Neyriz lavas. Sabzevar magmatic rocks plot above but near the Northern Hemisphere Reference Line on the $^{208}Pb/^{204}Pb$ vs. $^{206}Pb/^{204}Pb$ diagram (Fig. 7C). They plot between less radiogenic Oman lavas and more radiogenic subducted sediments, pointing to a greater contribution from subducted sediments to their mantle source.

6. Mineral composition

Mineral composition data for mantle peridotites and crustal cumulate gabbros are available in Supplementary Table 2.

6.1. Olivine

Olivine in mantle harzburgites and lherzolites has Forsterite and NiO contents ranging from 90.2 to 91.7 and from 0.35 to 0.42 wt.%, respectively, lower than in chromite-rich dunites (Fo = 94–95 and NiO = 0.45–0.50) (Supplementary Table 2A).

6.2. Spinel

Spinel in harzburgites shows constant Cr# (44-47), similar to SSZ-type and/or depleted abyssal peridotites, while in impregnated

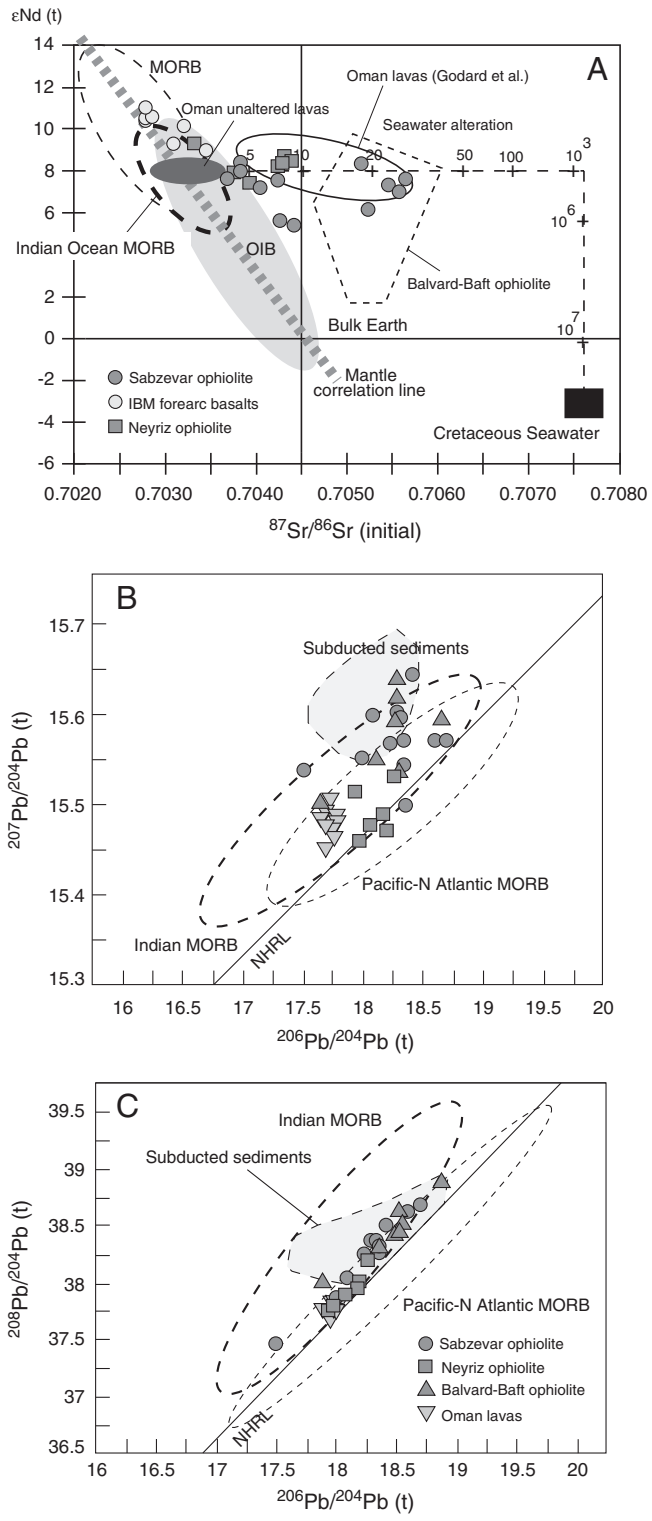

Fig. 7. εNd versus $^{87}Sr/^{86}Sr$ for the Sabzevar magmatic rocks, recalculated at 100 Ma. The dashed line indicates the effect of contamination by Cretaceous seawater for different water/rock ratios (modified after Godard et al., 2006). (B) $^{207}Pb/^{204}Pb$ and (C) $^{208}Pb/^{204}Pb$ against $^{206}Pb/^{204}Pb$ for Neyriz ophiolites (modified after Godard et al., 2006 and Liu et al., 2013). Data for Oman lavas are from Godard et al. (2006), Balvard–Baft ophiolite from Shafaii Moghadam et al. (2013a, 2013b, 2013c), Neyriz ophiolites from Moghadam et al. (2014) and IBM forearc basalts from Reagan et al. (2010).

lherzolites Cr# varies from 24 to 26. These spinels have low TiO_2 contents (0.01–0.04 wt.%) (Supplementary Table 2B). Both in Cr# vs. TiO_2 and in Cr# (spinel) vs. forsterite (olivine) diagrams, the harzburgite spinels are consistent with 15–17% partial melting of their peridotite host (Fig. 8A and B) while impregnated lherzolites have lower Cr# consistent with 10% partial melting. Dunite spinels show higher values of Cr# (68–69) and TiO_2 contents (0.05–0.08 wt.%).

6.3. Orthopyroxene

Harzburgite orthopyroxene has 89–92 Mg# and 1.9–2.6 wt.% Al_2O_3 with high Cr_2O_3 content (0.6–0.7 wt.%) (Supplementary Table 2D). Lherzolite orthopyroxene has higher Al_2O_3 content (2.7–3.9 wt.%). Orthopyroxene in gabbros has lower Mg# (75–83) and Al_2O_3 (1.2–1.8 wt.%) but higher TiO_2 (0.1–0.3 wt.%) and orthoferrosilite end-member (Fs = 0.17–0.24; bronzite).

6.4. Clinopyroxene

Harzburgite clinopyroxene has higher Mg# (93–94) and Al_2O_3 (2.7–3.2 wt.%) but lower TiO_2 (0–0.05 wt.%) (Supplementary Table 2C). Lherzolites have variable Al_2O_3 (1.9–4.5 wt.%) and TiO_2 (0.07–0.13 wt.%) contents. On a TiO_2 vs. Mg# diagram (Fig. 8C) they are similar to SSZ-peridotites. Gabbro clinopyroxene has lower Mg# (79–85) but higher TiO_2 (0.20–0.55 wt.%).

6.5. Plagioclase

Gabbro plagioclase is anorthite-rich (~An 89-92) (Supplementary Table 2E). In the clinopyroxene Mg# against anorthite content in plagioclase diagram, the samples plot as SSZ-type gabbros (Fig. 8D).

7. Biostratigraphy and TIMS U–Pb zircon dating

Pelagic limestones between the pillow lavas (both SSZ- and OIB-like types) have the following micro-faunas: *Contusotruncana fornicate*, *Globotruncana lapparenti*, *Globotruncanita stuarti*, *Globotruncana ventricosa*, indicating Late Campanian to Early Maastrichtian ages (~75–68 Ma) (A. Taheri, personal communications).

Three Sabzevar plagiogranitic rocks and one sample from Torbat-e-Heydarieh ophiolite have been dated by zircon U–Pb.

7.1. Sample SZ11-28 (Fig. 3)

This is a tonalitic dike that crosscuts diabasic dikes within mantle harzburgites (Figs. 3 and 4D). The sample has concave-upward REE pattern and a positive Eu anomaly, and shows negative Nb–Ti anomalies relative to N-MORB, resembling highly depleted tholeiitic or boninitic-like rocks (Fig. 6I and J). Its εNd (+7.9) is similar to other Sabzevar plagiogranites, lavas as well as diabase dikes. This dike may have formed by fractional crystallization of Sabzevar mafic melts.

Zircon in sample SZ11-28 occurs as euhedral short prismatic crystals with magmatic zoning (Appendix 3). The Th/U ratio of analyzed zircons is intermediate, between 0.43 and 0.47, consistent with a magmatic origin. Three analyses yield a mean $^{206}Pb/^{238}U$ age of 99.92 ± 0.12 Ma (Table 2). This age is interpreted to indicate the time of intrusion of the tonalite dike, in the early stages of Sabzevar ophiolite formation.

7.2. Sample SZ11-72 (Fig. 3)

This type of plagiogranite intrudes the sheeted dike complex (Fig. 3). It has an LREE-enriched pattern and is enriched in LILE and depleted in HFSE relative to N-MORB, similar to island-arc tholeiites (Fig. 6I and J).

Zircon occurs mainly as euhedral short prisms, with magmatic concentric zoning (Appendix 3), containing 488–748 ppm U and relatively high Th/U ratios of 0.59–0.74 (Table 2). The three analyses define a mean $^{206}Pb/^{238}U$ age of 90.16 ± 0.12 Ma (Fig. 9) interpreted as the time of emplacement of the plagiogranite.

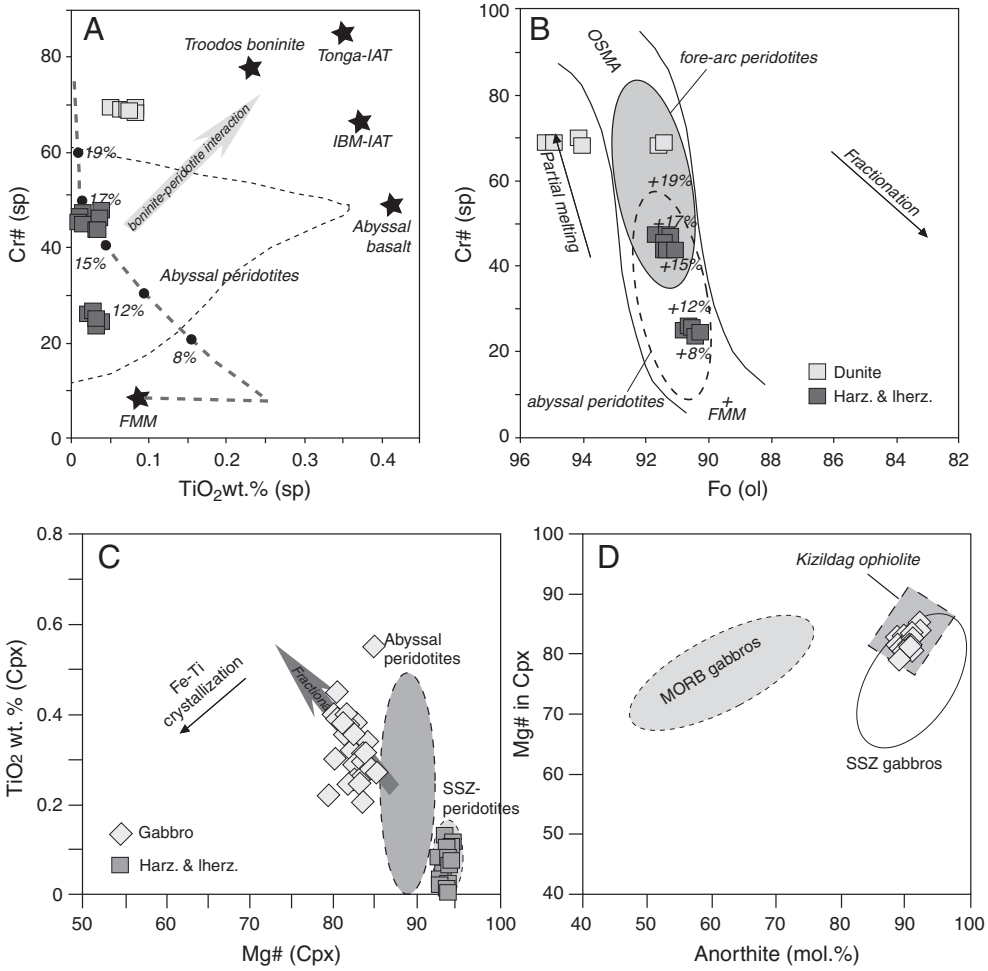

Fig. 8. A) Relation between Cr# and TiO_2 contents of spinel in mantle peridotites of the Sabzevar ophiolite. The thick gray arrow shows the effect of melts (with composition of Troodos boninites) on refractory subduction zone peridotites. Compositions of Tonga and Izu–Bonin–Mariana island arc tholeiites and abyssal basalts are from Pearce et al. (2000) and the composition of Troodos boninite is from Dick and Bullen (1984). B) Relation between Cr# values of spinels and Fo contents of olivine in equilibrium with spinel in Sabzevar mantle peridotites. FMM: fertile MOR mantle. Passive continental margin and abyssal peridotite fields are from Dick and Bullen (1984), forearc peridotite field is from Pearce et al. (2000). OSMA (olivine–spinel mantle array), partial melting and differentiation trends are from Arai (1994). C) Variation in Mg# value vs. TiO_2 contents of peridotite and gabbro clinopyroxene (abyssal and forearc peridotite fields are from Bedard et al., 2009). D) Anorthite content vs. clinopyroxene Mg# in the gabbroic rocks for the Sabzevar ophiolite. The Kizildag ophiolite data is from Bagcı et al. (2005). Fields of MORB and arc gabbro are from Burns (1985).

7.3. Sample SZ11-44

This sample is taken from a small plagiogranitic plug injected within coarse-grained crustal cumulate gabbros near the Sang-e-Sefid village (Fig. 3, Appendix 1). The rock has a flat REE pattern with an LILE enrichment and Nb and Ta depletion, indicating supra-subduction zone affinity (Fig. 6I and J). Its εNd value (+7.9) is similar to other Sabzevar plagiogranites, lavas as well as diabasic dikes. The Th/U ratio of analyzed zircons is high, between 1 and 1.75, consistent with a magmatic origin. Three of the four analyzed grains yield a mean $^{206}Pb/^{238}U$ age of 77.82 ± 0.28 Ma, while a fourth point is less precise and slightly older (79.68 ± 1.3 Ma). The age of 77.82 Ma records intrusion of the plagiogranitic plug in the late stages of development of the Sabzevar ophiolite.

7.4. Sample TH12-20

In order to check for age variations along the Sabzevar–Torbat-e-Heydarieh ophiolite belt, we took one sample from the Torbat-e-Heydarieh ophiolite. This sample is from a small plagiogranitic plug injected into medium to coarse-grained gabbros. Geochemical data (unpublished data) show that the rock has an island-arc tholeiitic signature.

The zircon population of this sample consists of a mix of long-prismatic and short-prismatic euhedral and well-zoned crystals (Appendix 3). The Th/U ratio of the analyzed zircons varies between 0.32 and 0.55. Four of the five analyzed zircon grains give a mean $^{206}Pb/^{238}U$ age of 98.40 ± 0.29 Ma whereas one point defines a younger age (97.8 ± 1.1 Ma) suggesting a slight resetting by Pb loss. The 98.40 ± 0.29 Ma age is taken to indicate the time of emplacement of the plagiogranitic plug and can be considered as approximating the formation age of the Torbat-e-Heydarieh ophiolite, which is similar to the maximum time of Sabzevar ophiolite formation.

8. Discussion

Below we use our new geochemical, isotopic, and geochronological results to examine three issues: 1) When did the Sabzevar ophiolite form? 2) What was the source of Sabzevar ophiolitic magmas, and how did these evolve? 3) What are the tectonic implications of these results?

8.1. Age of Sabzevar ophiolite and its significance

Sabzevar plagiogranites yield a range of Cretaceous U–Pb zircon ages at ~100, 90 and 78 Ma (Fig. 10), reflecting a protracted period of

Table 2
U–Pb data for zircon from Sabzevar ophiolites.

Zircon characteristics[1)]	Weight[2)] [mg]	U[2)] [ppm]	Th/U[3)]	Pbc[4)] [pg]	$^{206}Pb/^{204}Pb$[5)]	$^{207}Pb/^{235}U$[6)]	± 2s [abs]	$^{206}Pb/^{238}U$[6)]	±2s [abs]	Rho	$^{207}Pb/^{206}Pb$[6)]	±2s	$^{206}Pb/^{238}U$[6)] [Ma]	±2s	$^{207}Pb/^{235}U$[6)]	±2s
SZ11-28 plagiogranitic dike																
eu sp [16]	121	89	0.44	3.8	2819	0.10336	0.00032	0.015640	0.000033	0.78	0.04793	0.00009	100.04	0.21	99.9	0.3
eu sp [1]	35	123	0.47	1.5	2743	0.10337	0.00045	0.015617	0.000035	0.70	0.04801	0.00015	99.89	0.23	99.9	0.4
eu sp [21]	108	105	0.43	2.4	4676	0.10316	0.00034	0.015603	0.000035	0.78	0.04795	0.00010	99.81	0.22	99.7	0.3
SZ10-72 plagiogranite																
eu sp [1]	3	598	0.65	2.0	792	0.09335	0.00094	0.014091	0.000035	0.49	0.04805	0.00044	90.20	0.22	90.6	0.9
eu sp [10]	9	488	0.59	1.5	2659	0.09261	0.00048	0.014084	0.000034	0.61	0.04769	0.00020	90.16	0.22	89.9	0.4
eu sp [1]	3	748	0.74	1.2	1628	0.09305	0.00056	0.014079	0.000033	0.58	0.04794	0.00024	90.12	0.21	90.3	0.5
TH12-20 medium-grained plagiogranite																
eu tip [3]	15	82	0.32	6.9	192	0.1021	0.0021	0.015422	0.000041	0.31	0.04803	0.00094	98.66	0.26	98.7	1.9
eu tip [1]	10	109	0.55	2.3	470	0.1019	0.0016	0.015381	0.000047	0.46	0.04804	0.00070	98.40	0.30	98.5	1.5
eu lp [1]	2	259	0.43	1.9	274	0.1030	0.0030	0.015378	0.000042	0.58	0.04860	0.00132	98.38	0.27	99.6	2.7
eu tip [8]	30	111	0.34	3.6	917	0.10168	0.00066	0.015356	0.000034	0.56	0.04803	0.00027	98.24	0.22	98.3	0.6
eu sp [3]	13	99	0.35	1.8	710	0.1011	0.0012	0.015272	0.000041	0.47	0.04803	0.00051	97.71	0.26	97.8	1.1
SZ11-44 small plagiogranite plug injected into coarse-grained crustal gabbros																
fr [1]	<1	>110	1.75	4.9	36	0.083	0.018	0.01244	0.00020	0.42	0.048	0.010	79.68	1.30	81.0	16.6
eu sp [1]	<1	>220	1.57	1.1	178	0.0810	0.0038	0.012159	0.000057	0.53	0.0483	0.0021	77.91	0.37	79.1	3.6
fr [3]	<1	>30	1.00	1.0	39	0.061	0.030	0.01215	0.00024	0.58	0.037	0.018	77.87	1.54	60.5	28.5
eu tip [1]	<1	>230	1.09	1.4	142	0.0779	0.0050	0.012120	0.000073	0.54	0.0466	0.0029	77.66	0.46	76.2	4.7

1) eu = euhedral; sp = short prismatic; lp = long prismatic; fr = fragment; [1] = number of grains; all treated with chemical abrasion.
2) Weight and concentrations are known to be better than 10%, except for those near and below the ca. 1 μg limit of resolution of the balance.
3) Th/U model ratio inferred from 208/206 ratio and age of sample.
4) Pbc = total common Pb in sample (initial + blank).
5) Raw data corrected for fractionation.
6) Corrected for fractionation, spike, blank, initial common Pb and initial ^{230}Th disequilibrium (assuming Th/U magma = 4); error calculated by propagating the main sources of uncertainty.

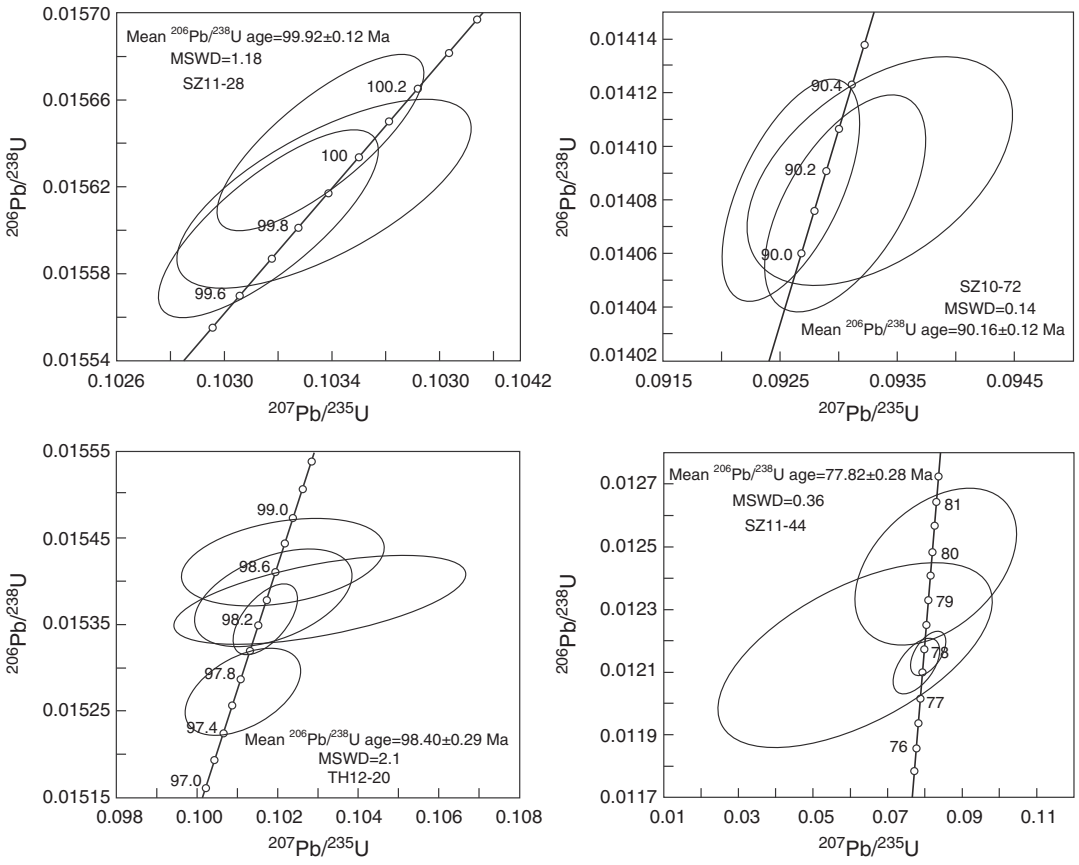

Fig. 9. Zircon concordia diagrams displaying U–Pb data from the Sabzevar plagiogranites.

formation of the ophiolitic units. A significant age range for this ophiolite is also indicated by the Campanian–Maastrichtian carbonate deposited between pillows. More data are needed to test if there was a continuum of activity for 20 m.y. or whether the evolution was episodic. Unfortunately most Sabzevar plagiogranites and gabbros lack zircon, making it difficult to test these possibilities today. Zircon and titanite from felsic segregations in mafic granulites and high-P rocks from the Sabzevar subduction channel yield U–Pb ages of 107.4 ± 2.4

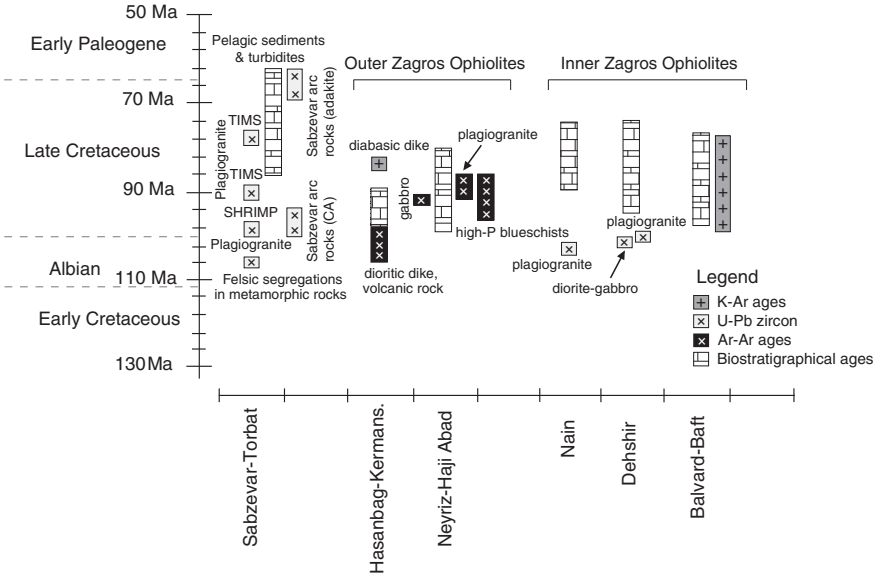

Fig. 10. Simplified chart showing the ages of magmatic and sedimentary sequences of the Sabzevar ophiolites. For comparison we also plotted data from Zagros ophiolites. Ar–Ar age data on the Hasanbag ophiolites (Iraq) from Ali et al. (2012); K–Ar ages on the Kermanshah ophiolite from Delaloye and Desmons (1980); Ar–Ar ages on Neyriz plagiogranites are from Lanphere and Pamic (1983) and on Neyriz gabbros from (Babaei et al., 2006). Ages of high pressure metamorphic rocks of the Haji Abad ophiolite are from Agard et al. (2006). K–Ar ages of inner belt Zagros ophiolites are from Shafaii Moghadam (2009) and U–Pb zircon ages of the Nain and Dehshir ophiolites are from Shafaii Moghadam et al. (2013b). U–Pb zircon data on Sabzevar arc rocks are from Shafaii Moghadam et al. (unpublished data).

and 105.9 ±2.3 Ma (Albian), respectively (Fig. 10; Rossetti et al., 2010). These ages show that subduction beneath the Sabzevar basin (Proto-Sabzevar Ocean) was active in Late Early Cretaceous time while 100 Ma old plagiogranites indicate that seafloor spreading – perhaps infant arc magmatism – was going on above this subduction zone. Younger (90–78 Ma) Sabzevar plagiogranites could reflect arc magmatism. These relationships strongly suggest that Sabzevar ophiolites are similar to the volcanic-arc type ophiolite of Dilek and Furnes (2011), where the crustal sequence rocks evolve through longer period of magmatism than expected at a mid-ocean ridge. However, the age of calc-alkaline granitoids SSE of the Sabzevar ophiolites (Fig. 2) is ca. 98–92 Ma (Moghadam et al., submitted for publication). These arc rocks crosscut the ophiolitic substratum and Torbat-e-Heydarieh ophiolites could represent a back-arc basin behind this arc. Younger calc-alkaline to adakitic arc magmatism in the SSE Sabzevar ophiolites peaked at ~60–68 Ma and 40–45 Ma (Moghadam et al., submitted for publication). Together, these ages indicate subduction initiation in the latest Early Cretaceous, infant arc magmatism and then mature intra-oceanic arc magmatism from ca. 100 to 78 Ma (Fig. 10). The younger arc rocks formed by magmatism after basin closure and could be related to the Tethyan subduction beneath Central Iran at ca. 40–45 Ma (Moghadam et al., submitted for publication). U–Pb zircon ages on the Sabzevar ophiolites are similar to those from the Zagros ophiolites (Fig. 10), except for the age of the younger plagiogranites.

8.2. Source nature and magma process

The geochemical characteristics described above indicate that Sabzevar magmatic rocks have both OIB- and SSZ-signatures (calc-alkaline, IAT and highly depleted tholeiite or boninitic-like). Some Sabzevar pillowed and massive lavas show OIB geochemical signature with high HFSE content and fractionated REE patterns. There is no systematic geographic or stratigraphic control on the distribution of these lava types, as far as we can tell; they are distributed randomly in the ophiolitic lava sequences. Sabzevar OIB-like lavas are similar to OIB-like lavas described from the Kermanshah, Kurdistan, Balvard–Baft and Haji–Abad ophiolites (Saccani et al., 2013, 2014; Moghadam and Stern, 2011). Saccani et al. (2014) proposed that Zagros ophiolitic OIB melts originated from 7% to 16% polybaric partial melting of an MORB-type mantle source that was enriched by plume-type components. Some studies suggest that Iranian ophiolitic OIB (e.g., Kermanshah and Kurdistan) formed during the early stage of oceanic formation (in Late Permian time) (Saccani et al., 2013, 2014) that correlates with the alkaline lavas of the Oman Hawasina complex (Robertson, 2007), formed during the rifting/early oceanization phase of north Gondwana. However, the Sabzevar OIB- and SSZ-type lavas can be observed in the field to be intercalated and both are associated with Upper Cretaceous pelagic limestones.

It is not clear how SSZ and OIB magmas were generated at the same time and erupted in the Sabzevar ophiolite. Subduction components provided from an underlying subducted slab should have affected the entire overlying mantle wedge, but it seems possible that at least some of the supra-subduction mantle is capable of escaping slab-related fluid ingress. The association of SSZ and OIB-type magmatism is also mentioned in other arc setting (e.g., Neill et al., 2013; Sorbadere et al., 2013). Sabzevar SSZ-type lavas have positive εNd(t) values (+6.1 to +8.3; except two samples with lower values; +5.4 and +5.6) and radiogenic Pb isotope ratios. These lavas show an affinity to an MORB source, contaminated by subduction-related components. Significant enrichment in LILEs and HFSE depletion with pronounced negative Nb–Ta anomalies for the Sabzevar ophiolites suggest addition of crustal components into the mantle source (Fan et al., 2010; Li et al., 2013; Tian et al., 2008). Their Sr–Nd–Pb isotopic compositions trend towards crustal/sedimentary components along the mantle array (Fig. 8), further indicating an MORB-like source with some addition of crustal components. Sabzevar ophiolitic OIB-type lavas were generated from a subduction component-free mantle, perhaps as a result of asthenosphere migration from beneath Eurasia. Interpretation of a distal source for OIB magmas is supported by the observed lack of intrusive OIB-type igneous rocks. As many of the OIB-like rocks are pillow lavas, the other scenarios for generation of these types of lavas may include slab tearing and ingress around the edge of a slab, or probably some intrinsic part of the subduction initiation process as ways to get small-degree melting of the most enriched mantle components underway.

Sabzevar magmatic rocks (except OIB-type lavas) plot between MORB and subduction-fluid metasomatized components in the $(Ta/La)_n$ vs. $(Hf/Sm)_n$ diagram (Fig. 11A). Addition of slab components usually contributes to lower εNd(t) values for the derived magmas (Fan et al., 2010; Li et al., 2013; Tian et al., 2008). The high Th and LREE content of the Sabzevar magmatic rocks relative to MORB, as well as high Pb isotopic ratios similar to those of global pelagic sediments, all argue for the involvement of subducted sediments in the mantle source of non-OIB Sabzevar igneous rocks. The εNd(t) vs. $^{206}Pb/^{204}Pb$ ratios show that the addition of less than 0.5% pelagic sediments into the MORB mantle source can explain the isotopic signature of Sabzevar SSZ igneous rocks (Fig. 11B), although some samples also show contributions of slab fluids. Most Sabzevar rocks (except OIB-type lavas) have higher Th/Yb and plot far away from mantle array and are similar to arc-related rocks (Fig. 11C). This is evidenced also in the Ce/Nb vs. Th/Nb diagram (Fig. 11D); the magmatic rocks have higher Th/Nb and Ce/Nb and resemble arc rocks, but differ from back-arc basin lavas.

The origin of plagiogranites in the Sabzevar ophiolites is also debatable. Ophiolitic plagiogranites are either products of shallow differentiation of basaltic magmas (e.g., Lippard et al., 1986; Rollinson, 2009) or reflect low-pressure melting of amphibolitic oceanic gabbros (e.g., Gillis and Coogan, 2002; Koepke et al., 2005; Rollinson, 2009). Sabzevar plagiogranites (except the highly depleted tholeiitic or boninitic-like ones that are injected into mantle) show REE patterns and isotopic similarities with basaltic rocks and therefore are related by fractional crystallization. The highly depleted tholeiitic (boninitic-like) plagiogranites have higher Mg# and Ni and are similar to the Wadi Hamaliya (Oman) plagiogranites described by Rollinson (2009). These rocks may be the fractionated products of (boninitic-like) melts formed by hydrous melting of mantle depleted harzburgites (Crawford et al., 1989).

8.3. Tectonic implications

The similarity between the Zagros and Sabzevar ophiolites ages shows that they may have similar origins but that Zagros ophiolites may be slightly older (ca. 103–99 Ma) than Sabzevar (ca. 100–78 Ma). Nearly all Late Cretaceous Neotethyan ophiolites are about the same age; 90–94 Ma for Troodos; 95 Ma for Oman; 91–92 Ma for Kizildag (Turkey); 92–98 Ma for Zagros Outer belt and 103–99 Ma for Inner belt ophiolites (see Shafaii Moghadam and Stern, 2011 for more explanation) suggesting magmatism over a shorter time than Sabzevar ophiolite; as expected from SSZ-type ophiolites (compared to volcanic arc-type). Most rocks from these ophiolites show SSZ geochemical signature.

The geochemical data in this study indicates that most Sabzevar lavas have SSZ or OIB geochemical signatures and that MORB-type lavas are rare. Most plutonic rocks, including plagiogranites, have highly depleted tholeiitic or boninitic-like characteristics. Mantle rocks also show SSZ signatures, as shown by spinel and pyroxene compositions.

SSZ-related lavas, plutonic rocks and mantle peridotites are abundant in the Sabzevar ophiolites. Our paleontological ages vary from Campanian to Maastrichtian (75–68 Ma) in the Sabzevar ophiolites. Sabzevar ophiolite plagiogranites have different ages, varying from ca. 100 to 78 Ma. These ages are comparable with U–Pb zircon ages on the plutonic rocks from S-SE of the Sabzevar ophiolites. The granitoid plutons in S-SE Sabzevar were emplaced from Cenomanian–Turonian (97.0 ± 0.2 Ma; 92.8 ± 1.3 Ma) to Oligo–Miocene (29.8 ±

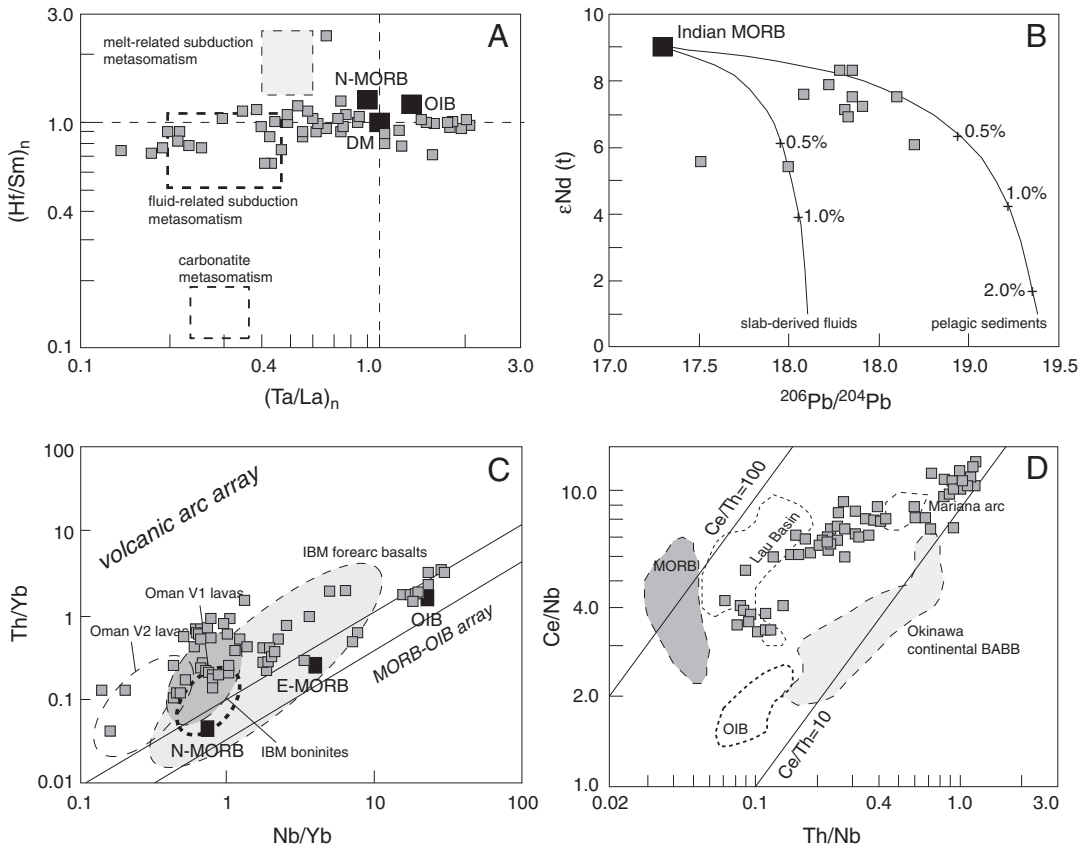

Fig. 11. $(Hf/Sm)_n$ vs. $(Ta/La)_n$, εNd vs. $^{206}Pb/^{204}Pb$ (Fan et al., 2010), Th/Yb vs. Ta/Yb (Pearce and Peate, 1995) and Ce/Nb vs. Th/Nb (Sandeman et al., 2006) variation diagrams for the Sabzevar magmatic rocks.

0.2 Ma) (Moghadam et al., submitted for publication; Alaminia et al., 2013). The late Cretaceous plutons have high positive εNd (similar to Sabzevar ophiolitic rocks), clearly issued from a depleted mantle source, and could be related to the subduction of the Sabzevar oceanic lithosphere (Proto-Sabzevar Ocean). Younger granitoids and lavas from this region have ages of ~40–42 Ma, similar to the main phase of the Urumieh–Doktar arc and may relate to the Tethyan subduction beneath the Central Iran (Moghadam et al., submitted for publication). The arc signature of the magmatic rocks from the Sabzevar ophiolite and >10 Ma U–Pb age differences between crustal rocks, as well as the presence of thick felsic plutons crosscutting the oceanic lithosphere show that these ophiolites resemble the volcanic arc-type ophiolite of Dilek and Furnes (2011).

All geochemical, geochronological as well as paleontologic evidence from the Sabzevar ophiolites indicate that the Sabzevar Ocean was open between the Lut Block to the south and the Binalud mountains (Turan block) to the north since at least mid-Cretaceous time (Fig. 12). This location places it in a back-arc basin position behind the Zagros convergent margin. The Sabzevar oceanic basin may have connected SW via the Nain ophiolite with the Zagros ophiolites, but it is very difficult to confirm or refuse this suggestion, as the intervening region is not well exposed. There are also no aeromagnetic data that could identify buried magnetic ophiolitic rocks. Regardless of how the Sabzevar oceanic basin opened, subduction began before Albian time, testified by the age of felsic segregations in the Sabzevar high-P metamorphic rocks. The intraoceanic subduction was responsible for generating the SSZ-related magmas within the Sabzevar oceanic lithosphere and nucleation and growth of a mature arc between the Sabzevar ophiolite to the north and Cheshmeshir and Torbat-e-Heydarieh ophiolites to the south-southeast. Evidence for oceanic lithosphere behind this arc comes from Oryan ophiolites. The volcano-pelagic series of the Oryan zone include Cenomanian to Maastrichtian deep sea pelagic sediments interbedded with pyroclastic and andesitic to dacitic lavas. This sequence grades upward into a series of Maastrichtian to Paleocene shallow water sediments and then into Oryan marine sediments (lower and middle Oryan sediments) from Early Eocene to early Middle Eocene time. This is the same also for the Torbat-e-Heydarieh ophiolite farther to the SE. Magmatic rocks with Eocene ages (ca. 40–42 Ma) north of the Dorouned fault may show a snapshot of continental arc magmatism after closure of the Sabzevar oceanic basin and should be related to Neotethyan Ocean subduction beneath Iran.

9. Conclusions

Geochronological and geochemical data indicate that the Sabzevar ophiolites formed from ~100 to 78 Ma encompassing an evolution from infant to mature arc stages. High LILEs and depletion in HFSEs as well as Nd–Pb isotopic signatures of the Sabzevar magmatic rocks indicate derivation of the magmas from a depleted MORB-type mantle contaminated by subducted components. The Sabzevar ophiolites represent an embryonic, subduction-related oceanic basin that was open between the Lut Block to the south and the Binalud mountains (Turan block) to the north since at least mid-Cretaceous time. Intraoceanic subduction was responsible for generating the SSZ-related magmas within the Sabzevar oceanic lithosphere and then nucleation and growth of a mature arc, testified by thick granitic crust within the Sabzevar substratum.

Supplementary data to this article can be found online at http://dx.doi.org/10.1016/j.lithos.2014.10.004.

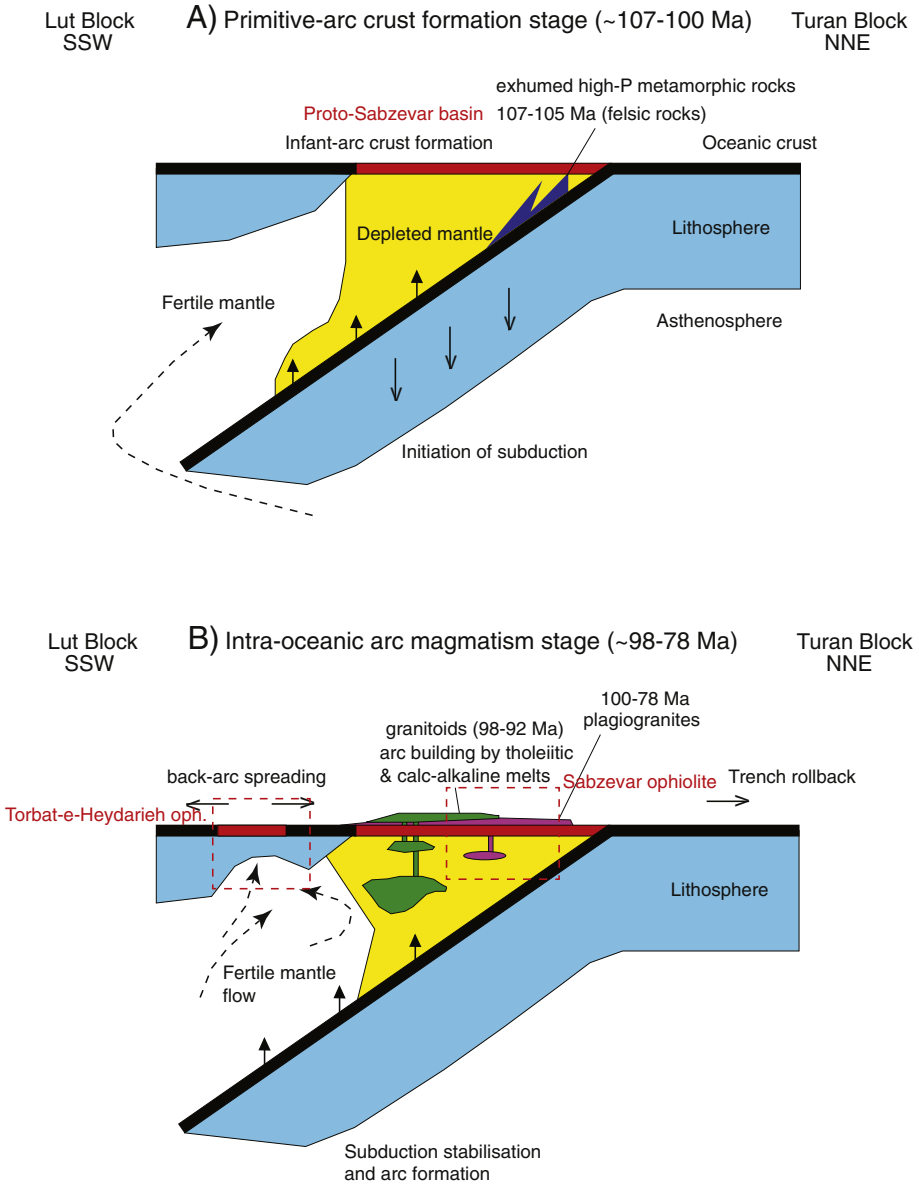

Fig. 12. Schematic models for the formation and evolution of the Sabzevar oceanic basin in NE Iran. A) Intra-oceanic subduction in mid-Cretaceous time; primitive arc crust formation in Late Cretaceous and exhumation of the high-P metamorphic rocks; B) formation of SSZ-related plagiogranite and other crustal rocks and crystallization of late Cretaceous granitoids (arc rocks). In this time, continuing rollback causes lateral upwelling of a fertile mantle diapir (DMM), which, in the presence of slab-derived fluids, melts to yield supra-subduction zone magmas. The stabilization of the magmatic front by continued subduction produces the migration of the locus of extension to a back-arc position, which resulted to the BABB-like magmatism of the Torbat-e-Heydarieh ophiolite (colored on-line).

Acknowledgments

We are very grateful to Sobhi Nasir and an anonymous reviewer for their constructive reviews of the manuscript. All logistical support during field studies came from Damghan University. We thank Federico Rossetti for providing EMP on Sabzevar rocks.

References

Agard, P., et al., 2006. Transient, syn-obduction exhumation of Zagros blueschists inferred from P–T-deformation-time and kinematic constraints: implications for Neotethyan wedge dynamics. Journal of Geophysical Research 111, B11401. http://dx.doi.org/10.1029/2005JB004103.

Alaminia, Z., Karimpour, M.H., Homam, M., Fimger, F., 2013. The magmatic record in the Arghash region (northeast Iran) and tectonic implications. International Journal of Earth Sciences http://dx.doi.org/10.1007/s00531-013-0897-1.

Ali, S.A., Buckman, S., Aswad, K.J., Jones, B.G., Ismail, S.A., Nutman, A.P., 2012. Recognition of Late Cretaceous Hasanbag ophiolite-arc rocks in the Kurdistan Region of the Iraqi Zagros suture zone: a missing link in the paleogeography of the closing Neotethys Ocean. Lithosphere 4, 395–410.

Arai, S., 1994. Compositional variation of olivine-chromain spinel in Mg-rich magmas as a guide to their residual spinel peridotites. Journal of Volcanology and Geothermal Research 59, 279–294.

Babaei, H.A., Babaei, A., Ghazi, A.M., Arvin, M., 2006. Geochemical, 40Ar/39Ar age, and isotopic data for crustal rocks of the Neyriz ophiolite, Iran. Canadian Journal of Earth Sciences 43, 57–70.

Bahroudi, Omrani, 1999. 1/100000 Geological map of Bashtin region. Geological Survey of Iran.

Bagcı, U., Parlak, O., Hock, V., 2005. Whole rock and mineral chemistry of cumulates from the Kızıldag (Hatay) ophiolite (Turkey): clues for multiple magma generation during crustal accretion in the southern Neotethyan Ocean. Mineralogical Magazine 69, 53–76.

Baroz, F., Macaudiere, J., 1984. La serie volcanosedimentaire du chainon ophiolitique de Sabzevar (Iran). Ofioliti 9, 3–26.

Baroz, F., Macaudier, J., Montigny, H., Noghreyan, M., Ohnenstetter, M., Rocci, G., 1983. Ophiolite and related formation in the central part of the Sbzevar rang (Iran) and possible geotectonic reconstructions. Geodynamic project (Geotraverse) in Iran. Geological Society of Iran Rep. No. 51.

Baroz, F., Macaudiere, J., Montigny, R., Noghreyan, M., Ohnenstetter, M., Rocci, G., 1984. Ophiolites and related formations in the central part of the Sabzevar (Iran) and

possible geotectonics reconstructions. Neues Jahrbuch für Geologie und Paläontologie (Abhandlungen) 168, 358–388.
Barrier, E., Vrielynck, B., 2007. Palaeotectonic maps of the Middle East. Tectono–sedimentary–palinspastic maps from Late Norian to Pliocene. 14 Maps. CGMW/CCGM, Paris.
Bedard, E., Hebert, R., Guilmette, C., Lesage, G., Wang, C.S., Dostal, J., 2009. Petrology and geochemistry of the Saga and Sangsang ophiolitic massifs, Yarlung Zangbo Suture Zone, Southern Tibet: evidence for an arc–back-arc origin. Lithos 113, 48–67.
Berberian, M., King, G.C.P., 1981. Towards a paleogeography and tectonic evolution of Iran. Canadian Journal of Earth Sciences 18, 210–265.
Burns, L.E., 1985. The Border Ranges ultramafic and mafic complex, south central Alaska: cumulate fractionates of island arc volcanics. Canadian Journal of Earth Sciences 22, 1020–1038.
Celik, O.F., Chiaradia, M., Marzoli, A., Billor, Z., Marschik, R., 2013. The Eldivan ophiolite and volcanic rocks in the İzmir–Ankara–Erzincan suture zone, Northern Turkey: geochronology, whole-rock geochemical and Nd–Sr–Pb isotope characteristics. Lithos 172–173, 31–46.
Chiaradia, M., 2009. Adakite-like magmas from fractional crystallization and melting assimilation of mafic lower crust (Eocene Macuchi arc, Western Cordillera, Ecuador). Chemical Geology 265, 468–487.
Coleman, R.G., 1977. Ophiolites: Ancient Oceanic Lithosphere. Springer-Verlag, New York.
Crawford, A.J., Falloon, T.J., Green, D.H., 1989. Classification, petrogenesis and tectonic setting of boninites. In: Crawford, A.J. (Ed.), Boninites and Related Rocks. Unwin Hyman, pp. 1–49.
Davidson, J., Turner, S., Handley, H., Macpherson, C., Dosseto, A., 2007. Amphibole "sponge" in arc crust? Geology 35, 787–790. http://dx.doi.org/10.1130/G23637A.1.
Delaloye, M., Desmons, J., 1980. Ophiolites and mélange terranes in Iran: a geochronological study and its paleotectonic implications. Tectonophysics 68, 83–111.
Desmons, J., Beccaluva, L., 1983. Mid-ocean ridge and island arc affinities in ophiolites from Iran: palaeographic implications. Chemical Geology 39, 39–63.
Dick, H.J.B., Bullen, T., 1984. Chromian spinel as a petrogenetic indicator in abyssal and Alpine-type peridotites and spatially associated lavas. Contributions to Mineralogy and Petrology 86, 54–76.
Dilek, Y., 2003. Ophiolite concept and its evolution. In: Dilek, Y., Newcomb, S. (Eds.), Ophiolite Concept and the Evolution Of Geological Thought: Boulder, Colorado. Geological Society of America Special Paper 373, pp. 1–16.
Dilek, Y., Furnes, H., 2011. Ophiolite genesis and global tectonics: geochemical and tectonic fingerprinting of ancient oceanic lithosphere. Geological Society of America Bulletin 123, 387–411.
Fan, W., Wang, Y., Zhang, A., Zhang, F., Zhang, Y., 2010. Permian arc–back-arc basin development along the Ailaoshan tectonic zone: geochemical, isotopic and geochronological evidence from the Mojiang volcanic rocks, Southwest China. Lithos 119, 553–568.
Gillis, K.M., Coogan, L.A., 2002. Anatectic migmatites from the roof zone of an ocean ridge magma chamber. Journal of Petrology 43, 2075–2095.
Godard, M., Dautria, J.M., Perrin, M., 2003. Geochemical variability of the Oman ophiolite lavas: relationship with spatial distribution and paleomagnetic directions. Geochemistry, Geophysics, Geosystems (G) 4, 8609. http://dx.doi.org/10.1029/2002GC000452.
Godard, M., Bosch, D., Einaudi, F., 2006. A MORB source for low-Ti magmatism in the Semail ophiolite. Chemical Geology 234, 58–78.
Hart, S.R., 1984. A large-scale isotope anomaly in the Southern Hemisphere mantle. Nature 309, 753–757.
Kawahata, H., Nohara, M., Ishizuka, H., Hasebe, S., Chiba, H., 2001. Sr isotope geochemistry and hydrothermal alteration of the Oman ophiolite. Journal of Geophysical Research 106, 11083–11099.
Knipper, A., Ricou, L.E., Dercourt, J., 1986. Ophiolites as indicators of the geodynamic evolution of the Tethyan ocean. Tectonophysics 123, 213–240.
Koepke, J., Feig, S.T., Snow, J., 2005. Hydrous partial melting within the lower oceanic crust. Terra Nova 16, 286–291.
Lanphere, M.A., Pamic, T., 1983. 40Ar/39Ar ages and tectonic setting of ophiolites from Neyriz area, southeast Zagros range, Iran. Tectonophysics 96, 245–256.
Larocque, J., Canil, D., 2010. The role of amphibole in the evolution of arc magmas and crust: the case from the Jurassic Bonanza arc section, Vancouver Island, Canada. Contributions to Mineralogy and Petrology 159, 475–492.
Lensch, G., Mihm, A., Alavi-Tehrani, N., 1980. The post-ophiolitic volcanics north of Sabzevar (Iran): geology, petrography and major elements geochemistry. Neues Jahrbuch für Geologie und Paläontologie (Monatsheft) 11, 686–702.
Li, L., Lina, S., Xingd, G., Davise, D.W., Davisf, W.J., Xiao, W., Yina, C., 2013. Geochronology and geochemistry of volcanic rocks from the Shaojiwa Formation and Xingzi Group, Lushan area, SE China: implications for Neoproterozoic back-arc basin in the Yangtze Block. Precambrian Research 238, 1–17.
Lippard, S.J., Shelton, A.W., Gass, I.G., 1986. The ophiolite of northern Oman. Geological Society of London Memoir 11. Blackwell Scientific, Oxford (230 pp.).
Liu, J.F., Li, J.Y., Chi, X.G., Qu, J.F., Hu, Z.C., Fang, S., Zhang, Z., 2013. A late-Carboniferous to early early-Permian subduction-accretion complex in Daqing pasture, southeastern Inner Mongolia: evidence of northward subduction beneath the Siberian paleoplate southern margin. Lithos 177, 285–296.
Majidi, 1987. 1/100000 Geological map of Sabzevar region. Geological Survey of Iran.
McCulloch, M.T., Gregory, R.T., Wasserburg, G.T., Taylor, H.P., 1981. Sm–Nd, Rb–Sr, and 18O/16O isotopic systematics in an oceanic crustal section: evidence from the Samail ophiolite. Journal of Geophysical Research 86, 2721–2735.
McDonough, W.F., Sun, S.S., 1995. The composition of the Earth. Chemical Geology 120, 223–253.
Moghadam, H.S., Stern, R.J., 2011. Geodynamic evolution of Upper Cretaceous Zagros ophiolites: formation of oceanic lithosphere above a nascent subduction zone. Geological Magazine 148, 762–801.
Moghadam, H.S., Zaki Khedr, M., Chiaradia, M., Stern, R.J., Bakhshizad, F., Arai, S., Ottley, C. J., Tamura, A., 2014. Supra-subduction zone magmatism of the Neyriz ophiolite, Iran: constraints from geochemistry and Sr-Nd-Pb isotopes. International Geology Review 56, 1395–1412.
Moghadam, H.S., Li, X.-H., Ling, X.-X., Santos, J.F., Stern, R.J., Ling, Q.-L., Ghorbani, G., submitted for publication. Eocene Kashmar granitoids (NE Iran): Petrogenetic constraints from major and trace elements, U-Pb zircon geochronology, zircon Hf-O and whole rock Sr-Nd isotopes. Lithos (paper revised).
Neill, I., Kerr, A., Hastie, A., Pindell, J.L., Millar, I.L., 2013. The Albian–Turonian island-arc rocks of Tobago, West Indies: geochemistry, petrogenesis and Caribbean plate tectonics. Journal of Petrology 54, 1607–1639.
Noghreyan, M.K., 1982. Evolution geochimique, mineralogique et structurale d'un edifice ophiolitique singulier: le massif de Sabzevar (partie centrale), NE de l'IranThese Doc d'Etat, Universite de Nancy, France.
Nozaem, R., Mohajjel, M., Rossetti, F., Seta, M.D., Vignaroli, G., Yassaghi, A., Salvini, F., Eliassi, M., 2013. Post-Neogene right-lateral strike–slip tectonics at the northwestern edge of the Lut Block (Kuh-e–Sarhangi Fault), Central Iran. Tectonophysics 589, 220–233.
Ohnenestetter, M., Sider, H., 1982. Contraintes geochimiques apportees par le magmatisme sur le developpement du bassin marginal ensialique du Beaujolais au Devonian. Bulletin de la Societe Geologique de France 8 (IV), 499–510 (3).
Omrani, H., Moazzen, M., Oberhansli, R., Altenberger, U., Lange, M., 2013. The Sabzevar blueschists of the North-Central Iranian micro-continent as remnants of the Neotethys-related oceanic crust subduction. International Journal of Earth Sciences 102, 1491–1512. http://dx.doi.org/10.1007/s00531-013-0881-9.
Pearce, J.A., 2008. Geochemical fingerprinting of oceanic basalts with applications to ophiolite classification and the search for Archean oceanic crust. Lithos 100, 14–48. http://dx.doi.org/10.1016/j.lithos.2007.06.016.
Pearce, J.A., 2014. Immobile element fingerprinting of ophiolites. Elements 10, 101–108.
Pearce, J.M., Peate, D.W., 1995. Tectonic implications of the composition of volcanic arc magmatism. Annual Review of Earth and Planetary Sciences 23, 251–285.
Pearce, J.A., Barker, P.F., Edwards, S.J., Parkinson, I.J., Leat, P.T., 2000. Geochemistry and tectonic significance of peridotites from the South Sandwich arc-basin systems, South Atlantic. Contributions to Mineralogy and Petrology 139, 36–53.
Reagan, M.K., Ishizuka, O., Stern, R.J., Kelley, K.A., Ohara, Y., Blichert-Toft, J., Bloomer, S.H., Cash, J., Fryer, P., Hanan, B.B., Hickey-Vargas, R., Ishii, T., Kimura, J.I., Peate, D.W., Rowe, M.C., Woods, M., 2010. Fore-arc basalts and subduction initiation in the Izu–Bonin–Mariana system. Geochemistry, Geophysics, Geosystems (G3) 11, Q03X12. http://dx.doi.org/10.1029/2009GC002871.
Robertson, A.H.F., 2007. Overview of tectonic settings related to the rifting and opening of Mesozoic ocean basins in the Eastern Tethys: Oman, Himalayas and Eastern Mediterranean regions. In: Karner, G.D., Manatschal, G., Pinheiro, L.M. (Eds.), Imaging, Mapping and Modeling Continental Lithosphere Extension and Breakup. Geological Society of London, Special Publication no. 282, pp. 325–388.
Rollinson, H., 2009. New models for the genesis of plagiogranites in the Oman ophiolite. Lithos 112, 603–614.
Rossetti, F., Nasrabady, M., Vignaroli, G., Theye, T., Gerdes, A., Razavi, S.M.H., Moin Vaziri, H., 2010. Early Cretaceous migmatitic mafic granulites from the Sabzevar range (NE Iran): implications for the closure of the Mesozoic peri-Tethyan oceans in central Iran. Terra Nova 22, 26–34.
Saccani, E., Allahyari, K., Beccaluva, L., Bianchini, G., 2013. Geochemistry and petrology of the Kermanshah ophiolites (Iran): implication for the interaction between passive rifting, oceanic accretion, and OIB-type components in the southern Neo-Tethys Ocean. Gondwana Research 24, 392–411.
Saccani, E., Allahyari, K., Rahimzadeh, B., 2014. Petrology and geochemistry of mafic magmatic rocks from the Sarve–Abad ophiolites (Kurdistan region, Iran): evidence for interaction between MORB-type asthenosphere and OIB-type components in the southern Neo-Tethys Ocean. Tectonophysics http://dx.doi.org/10.1016/j.tecto.2014.02.011.
Sandeman, H.A., Hanmer, S., Tella, S., Armitage, A.A., Davis, W.J., Ryand, J.J., 2006. Petrogenesis of Neoarchaean volcanic rocks of the MacQuoid supracrustal belt: a back-arc setting for the northwestern Hearne subdomain, western Churchill Province, Canada. Precambrian Research 144 (1/2), 126–139.
Sengor, A.M.C., 1990. A new model for the late Palaeozoic–Mesozoic tectonic evolution of Iran and implications for Oman. In: Robertson, A.H.F., Searle, M.P., Ries, A.C. (Eds.), The Geology and Tectonics of the Oman Region. Geological Society of London, Special Publication no. 49, pp. 797–831.
Shafaii Moghadam, H., 2009. The Nain–Baft Ophiolites (Central Iran): Age, Structure and OriginPh.D. thesis Shahid Beheshti University, Tehran, Iran (532 p.).
Shafaii Moghadam, H., Stern, R.J., 2011. Geodynamic evolution of upper Cretaceous Zagros ophiolites: formation of oceanic lithosphere above a nascent subduction zone. Geological Magazine 148, 762–801.
Shafaii Moghadam, H., Stern, R.J., Chiaradia, M., Rahgoshay, M., 2013a. Geochemistry and tectonic evolution of the Late Cretaceous Gogher–Baft ophiolite, central Iran. Lithos 16–169, 33–47.
Shafaii Moghadam, H., Corfu, F., Stern, R.J., 2013b. U–Pb Zircon ages of Late Cretaceous Nain–Dehshir ophiolite, Central Iran. Journal of the Geological Society London 170, 175–184.
Shafaii Moghadam, H., Zaki Khedr, M., Arai, S., Stern, R.J., Ghorbani, G., Tamura, A., Ottley, C., 2013c. Arc-related harzburgite–dunite–chromitite complexes in the mantle section of the Sabzevar ophiolite, Iran: a model for formation of podiform chromitites. Gondwana Research http://dx.doi.org/10.1016/j.gr.2013.09.007.
Shervais, J.W., 1982. Ti–V plots and the petrogenesis of modern and ophiolitic lavas. Earth and Planetary Science Letters 59, 101–118.
Shojaat, B., Hassanipak, A.A., Mobasher, K., Ghazi, A.M., 2003. Petrology, geochemistry and tectonics of the Sabzevar ophiolite, north central Iran. Journal of Asian Earth Sciences 21, 1053–1067.

Sorbadere, F., Schiano, P., Metrich, N., Bertagnini, A., 2013. Small-scale coexistence of island-arc and enriched-MORB type basalts in the central Vanuatu arc. Contributions to Mineralogy and Petrology 166, 1305–1321.

Sun, S.S., Mcdonough, W.F., 1989. Chemical and isotopic systematics of oceanic basalts: implications for mantle composition and processes. In: Saunders, A.D., Norry, M.J. (Eds.), Magmatism in the Ocean Basins. Geological Society, London, Special Publications 42, pp. 313–345.

Tian, L.Y., Castillo, P.R., Hawkins, J.W., Hilton, D.R., Hanan, B.B., Pietruszka, A.J., 2008. Major and trace element and Sr–Nd isotope signatures of lavas from the Central Lau Basin: implications for the nature and influence of subduction componentsin the back-arc mantle. Journal of Volcanology and Geothermal Research 178, 657–670.